

Manuscript Details

Manuscript number	EARTH_2019_302
Title	Weathering indices as climate proxies. A step forward based on Congo and SW African river muds
Article type	Review Article

Abstract

Because weathering processes at the Earth's surface are controlled primarily by climate, a measure of weathering intensity determined from soils or sediments should be able to infer the climatic conditions associated with their formation. Available geochemical and mineralogical data on modern fluvial and marine muds from different regions of southern Africa and its Atlantic continental margin are used to review the links between sediment composition and climatic properties together with the possible causes of variance. Although river muds may not be generated exclusively in a single sedimentary cycle and erosion and weathering processes do not necessarily take place in a spatially homogeneous way, significant relationships between mineralogical and geochemical signatures of river mud and rainfall in the corresponding catchment area were recognised. Our study shows that the composition of clay is strongly influenced by climatically-driven weathering, whilst coarser mud fractions tend to be more affected by provenance, grain size, hydraulic sorting, and recycling. In the marine environment the climatic signal may be lost even in clay, because of hydraulic fractionation, authigenic mineral growth and mixing with foreign particles. Given the ubiquitous character of fluvial muds, and the easy and non-expensive methods available for separating and analysing clay fractions, their geochemical fingerprints represent a most precious source of information concerning climate. Any geochemical parameter used as a regional proxy of climate, however, still requires that the diversity of geological, geomorphological, and biological factors that affect its value are cautiously considered.

Keywords	Chemical weathering; Mud composition; Climate; SW African margin; Congo; Rainfall proxies
Corresponding Author	Pedro Dinis
Corresponding Author's Institution	University of Coimbra
Order of Authors	Pedro Dinis, Eduardo Garzanti, Annette Hahn, Pieter Vermeesch, Marina Cabral Pinto
Suggested reviewers	hilmar von eynatten, Youngsook Huh, Shouye Yang, Michael Babechuk, Jerome Gaillardet

1 **Weathering indices as climate proxies. A step forward based on Congo and SW**

2 **African river muds**

3

4 Pedro A. Dinis^{1*}, Eduardo Garzanti², Annette Hahn³, Pieter Vermeesch⁴, Marina C.
5 Pinto⁵

6 ¹ MARE - Marine and Environmental Sciences Centre, Department of Earth Sciences,
7 University of Coimbra, 3030- 790 Coimbra, Portugal

8 ² Laboratory for Provenance Studies, Department of Earth and Environmental Sciences,
9 University of Milano-Bicocca, 20126, Milano, Italy

10 ³ MARUM Center for Marine Environmental Sciences, University of Bremen, Bremen,
11 Germany

12 ⁴ University College London, London, WC1E 6BT, UK

13 ⁵ Geobiotec Research Centre; Department of Geosciences of University of Aveiro,
14 3810-193 Aveiro, Portugal

15

16 * Corresponding author: pdinis@dct.uc.pt

17

18

19 **Abstract:** Because weathering processes at the Earth's surface are controlled primarily
20 by climate, a measure of weathering intensity determined from soils or sediments
21 should be able to infer the climatic conditions associated with their formation.
22 Available geochemical and mineralogical data on modern fluvial and marine muds
23 from different regions of southern Africa and its Atlantic continental margin are used
24 to review the links between sediment composition and climatic properties together
25 with the possible causes of variance. Although river muds may not be generated
26 exclusively in a single sedimentary cycle and erosion and weathering processes do not
27 necessarily take place in a spatially homogeneous way, significant relationships
28 between mineralogical and geochemical signatures of river mud and rainfall in the
29 corresponding catchment area were recognised. Our study shows that the composition
30 of clay is strongly influenced by climatically-driven weathering, whilst coarser mud
31 fractions tend to be more affected by provenance, grain size, hydraulic sorting, and
32 recycling. In the marine environment the climatic signal may be lost even in clay,
33 because of hydraulic fractionation, authigenic mineral growth and mixing with foreign
34 particles. Given the ubiquitous character of fluvial muds, and the easy and non-
35 expensive methods available for separating and analysing clay fractions, their
36 geochemical fingerprints represent a most precious source of information concerning
37 climate. Any geochemical parameter used as a regional proxy of climate, however, still
38 requires that the diversity of geological, geomorphological, and biological factors that
39 affect its value are cautiously considered.

40 **Keywords:** Chemical weathering; Mud composition; Climate; SW African margin;
41 Congo; Rainfall proxies

1. Introduction

Paleo-climate records from continental settings are crucial to test the performance of general circulation models and to understand forcing factors of different components of the climate system. Stable isotopes from carbonate and phosphate obtained in tests of benthic and planktonic foraminifera, teeth and molluscs shells retrieved from marine sedimentary rocks have been widely used as sources of quantitative information about climatic variables (Grossman and Ku, 1996; Kobashi et al., 2001; Zachos et al., 2001). But the correlation of the marine climatic signal with the environmental conditions in the continent can be difficult to perform and cause biased interpretations of continental climate (Alroy et al., 2000). The quest for climatic proxies in continental realms has shown that isotope data determined in mammals' teeth and bones (Grimes et al., 2008; Bernard et al., 2009; Royer et al., 2013), speleothems (McDermott, 2004), fresh-water biota (Schmitz and Andreasson, 2001), vegetal remains (Diefendorf et al., 2010), authigenic lake sediments (Leng and Marshal, 2004) and other materials are able to provide robust information on local environmental conditions. However, speleothems are found only in very specific settings and the organic components are not always present or sufficiently well preserved in continental deposits to make accurate isotopic analysis.

Siliciclastic deposits can be regarded as excellent archives of past environmental conditions, the composition of finer-grained units being particularly suitable for climatic reconstructions (e.g., Dinis et al., 2017; Guo et al., 2018). The postulated links between

65 mud composition and climate are grounded on the fact that most fine-grained sediment
 66 carried in suspension is eroded soil derived from the source areas whose mineralogy
 67 and geochemistry, namely the levels of depletion in mobile elements relative to parent
 68 rocks, are largely dependent on weathering intensity (Viers et al., 2009). Furthermore,
 69 weathering rate has a crucial role in feedback mechanisms of the climate system (Walker
 70 et al., 1981; Berner et al., 1983), making its investigations particularly pertinent. A
 71 reliable climate proxy based on the geochemical and mineralogical composition of the
 72 widespread worldwide river mud deposits would thus allow a much broader
 73 understanding of past climatic conditions in continental settings. Unfortunately, the
 74 interpretation of the climatic control on the composition of muds is not a
 75 straightforward task. It can be considered that mud geochemistry and mineralogy are
 76 controlled by many diverse factors so that the role of climate will be hard to isolate. But,
 77 the widely used stable-isotope data are also affected by numerous analytical, biological
 78 and physical constraints, being strongly influenced by pH, salinity and diagenesis, not
 79 necessarily reflecting faithfully climatic parameters at the time of deposition (Leng and
 80 Marshal, 2004; Jaffrés et al., 2007; Grossman, 2012; Wierzbowski et al., 2013).

81 The present research arises from previous works focused on the weathering influence
 82 on the mineralogy and geochemistry of present-day river mud deposits from equatorial
 83 to sub-tropical southern Africa (Garzanti et al., 2013, 2014; Dinis et al., 2017).
 84 Complementing earlier approaches, we extend here the set of river mud samples,
 85 including marine muds collected offshore of the Congo river-mouth, and consider also
 86 geochemical data for the clay fraction. Ultimately, compositional data obtained for
 87 different silt and clay size fractions are tested as regional proxies of climatic variables.
 88 We also show how other exogenous factors may control mud composition and discuss

89 opportunities to minimize biased climatic interpretations grounded on the composition
 90 of mud deposits.
 91
 92 2. Linking weathering with climate
 93
 94 2.1 Weathering intensities versus weathering rates
 95 Weathering rate reflects the dissolution of bedrock by surficial fluids and removal of ions
 96 in solution and is usually expressed as the amount of mobilised material per units of
 97 area and time (von Blanckenburg et al., 2005). The intensity of weathering processes
 98 associated with soils and sediments is frequently assessed by ratios of the
 99 concentrations of elements or sets of elements that respond differently to chemical
 100 decomposition on the Earth's surface (see below). There is a global agreement that the
 101 intensity of chemical weathering largely depends on climate, being higher in warmer
 102 and more humid settings. Several authors also postulate that the rate of mineral
 103 decomposition at watershed scale depends on climate, increasing with temperature
 104 following the Arrhenius equation (Bradly and Carrol, 1994; White and Blum, 1995;
 105 Dessert et al., 2003). In this equation temperature is a power variable responsible for
 106 doubling the rate of the reaction for each 10°C rise. In addition, the influence of
 107 temperature on weathering rates seems to depend on precipitation, being substantially
 108 higher in more humid watersheds (White and Blum, 1995). Hence, one may expect that
 109 the flux of material generated during exogenous alteration must be higher in warm and
 110 humid tropical settings.

111 However, there is no consensus about the effective role of climate on weathering rates.
 112 While some argue that temperature and precipitation/runoff exert a strong influence
 113 (White and Blum, 1995; West et al., 2002), others showed that the exposure of fresh
 114 material is probably the most important controlling factor (Huh and Edmond, 1999;
 115 Oliva et al., 2003). In either case, physical denudation rates must exert a fundamental
 116 control on weathering intensity (Riebe et al., 2004; West et al., 2005; Gabet and Mudd,
 117 2009). In slowly eroding settings surface sediment suffers intense weathering before
 118 removal and the rate of weathering is limited by the supply of fresh material ("supply-
 119 limited" conditions). When the erosion rate is high the rate of weathering tends to be
 120 limited by the kinetics of the surface reactions, the so-called "weathering-limited"
 121 (Riebe et al., 2004) or "kinetic-limited" (West et al., 2005) conditions, and depends on
 122 the time available for weathering reactions and the kinetic of the reaction, which is
 123 controlled by temperature, water supply and vegetation cover (West et al., 2005). A
 124 weak relation between climatic variables and weathering can be detected, but just after
 125 removing the effects of physical denudations, which plays a dominant role (Dupré et al.,
 126 2003; Riebe 2004; von Blanckenburg, 2005).
 127 Weathering profiles are expected to be thicker and their upper levels more depleted in
 128 mobile elements in wetter and warmer environments, hence revealing higher
 129 weathering intensities. But a thick regolith cover will limit weathering rates because
 130 freshly exposed material tends to weather more rapidly than the old material that is
 131 already depleted in the most reactive components, explaining the high weathering rates
 132 in watersheds under strong denudation stress (Riebe et al., 2004; Gabet and Mudd,
 133 2009) or in dry/cold settings influenced by mechanical break-down due to frost action
 134 (Huh, 2003; Gabet et al., 2010). This is why, at a global scale, an increase in weathering

rate is expected when frost action becomes effective and low rates occur in warm/humid regions with thick regolith sequences (Huh, 2003). As summarized by Humphreys and Wilkinson (2007), soil production may either decrease exponentially with soil thickness or reach maximum at a certain soil thickness while decreasing towards lower and higher values, being invariably low in regions with thick regolith. High weathering rates in areas under rapid denudation covered by thin soil accounts for the inverse relation between suspend load and weathering intensity in big rivers (Gaillardet et al., 1999). From the previous discussion it is clear that weathering rate does not reflect climatic conditions as weathering intensity.

2.2 Proxies of weathering intensity

The intensity of chemical weathering affecting a specific region can be estimated through diverse weathering indices computed on the basis of the composition of soils and sedimentary deposits (Table 1). Since the definition of the Weathering Index of Parker (WIP; Parker, 1970) and, in particular, of the Chemical Index of Alteration (CIA; Nesbitt and Young, 1982), the chemical composition has been widely used to infer paleoclimate (e.g., Kalm et al., 1996; Ehrmann, 1998; Hodell et al., 1999; Hong et al., 2007; Liu et al., 2014; Clift et al., 2014; Hessler et al., 2017). The CIA is probably the most popular geochemistry weathering index, although other are commonly used as well, namely the Chemical Index of Weathering (CIW; Harnois, 1988), the Plagioclase Index of Alteration (PIA; Fedo et al., 1995), the Chemical Proxy of Alteration (CPA; Buggle et al., 2011) and the modified CIA index (CIX; Garzanti et al., 2014). Overviews of the rationale of these weathering indices were presented in previous studies (Price and Veldel, 2003;

Sheldon and Tabor, 2009; Guo et al., 2018). The alternatives to CIA were proposed to overcome recognised drawbacks on its application, such as the non-consistent behaviour of K during weathering (Harnois, 1988; Maynard, 1992), the occurrence of K-metasomatism/illitization (Fedo et al., 1995; Buggle et al., 2011), and the difficulties in establishing carbonate bound CaO (Buggle et al., 2011; Garzanti and Resentini, 2016). All of these parameters estimate weathering intensity based on the molar proportions of silicate-bound major elements. Except for WIP, where the value of the index is proportional to the concentration of mobile elements, they rely on a ratio between the non-mobile element Al (Al_2O_3 minus K_2O in PIA) and a set of non-mobile components that tend to be leached during feldspar weathering. Hence the value of the index tends to increase with weathering intensity.

Because most of these compositional parameters provide no information about the fate of Fe and Mg, which are preferentially hosted in olivine, amphibole, and pyroxene, other procedures were proposed to estimate weathering intensity affecting source rocks with these elements. The Mafic Index of Weathering ($\text{MIA}_{(o)}$ and $\text{MIA}_{(r)}$; Babechuck et al., 2014) is defined in a similar way as the CIA, but includes Fe in the group of mobile elements if the environment is reduced or added to Al in an oxidative environment. Additional multi-element approaches were also proposed. Using a Principal Component Analysis (PCA) applied to igneous rocks and their weathering products, Ohta and Arai (2007) defined a Mafic-Felsic-Weathering ternary diagram (MFW) in which the values for each vertex are obtained through mathematical expressions based on the weight percentage of major elements (SiO_2 , Al_2O_3 , Fe_2O_3 , TiO_2 , MgO , K_2O , Na_2O and silicate-bound CaO). It is proposed that the way samples plot in this diagram reflects the relative contribution of mafic/felsic source rocks and the weathering intensity. The

diagram $M^{+}-4Si-R^{2+}$ of Meunier et al. (2013) is also intended to tackle the problem of different source-rock composition and weathering intensity with a ternary diagram. Here composition is expressed as monocationic millimoles ($M^{+}=Na^{+}+K^{+}+2Ca^{2+}$; $4Si=Si/4$; $R^{2+}=F^{2+}+Mg^{2+}$). Sediments derived from felsic to ultra-mafic rocks appear in different fields parallel to the $M^{+}-R^{2+}$ border, and weathering intensity progresses towards the kaolinite pole represented by the $4Si$ vertex.

Many other ratios between two elements with different mobility were used as proxies of weathering intensity, including K_2O/Al_2O_3 and Na_2O/Al_2O_3 (Gallet et al., 1995), Th/U (Gu et al., 2002), Th/K (Deconinck et al., 2003), K/Na and Rb/Sr (Yang et al., 2004), Cs/Ti and Rb/Ti (Yan et al., 2007), and Rb/K (Roy et al., 2008). These ratios are not always applicable, for instance where the value is lower than in the UCC (Upper Continental Crust) standard (e.g., Th/U), or where weathering is too strong (e.g., K/Na and Rb/Sr) or too weak (e.g., K_2O/Al_2O_3 , K_2O/Th , Rb/K) (see above mentioned references for each parameter). Gaillardet et al. (1999) defined weathering indices α_E for different mobile elements by comparing their concentrations with that of a non-mobile element with similar magmatic compatibility. Alfa indices were thus defined as the ratio between a non-mobile and a mobile element normalised by the same ratio in the UCC (e.g., $\alpha_{Mg}=[Al/Mg]_{sample}/[Al/Mg]_{UCC}$; $\alpha_{Na}=[Sm/Na]_{sample}/[Sm/Na]_{UCC}$). With the exception of Al, the suggested non-mobile elements (Ti, Th, Sm and Nd) are strongly affected by the sorting processes that control heavy-mineral concentration (Garzanti et al., 2009). Hence, to avoid the bias introduced by hydraulic sorting, Garzanti et al. (2013) suggested referring all elements to Al (α_E^{Al}), which is hosted in minerals with different density (e.g. feldspar and garnet) and shape (e.g., tectosilicates and phyllosilicates). When dealing with source areas that are not akin to the UCC, such as volcanic islands or continental

206 flood basalts, different appropriate reference materials (e.g., average composition of
207 volcanic source rocks) should be used to establish the levels of depletion (Garzanti et al.,
208 2013; Dinis et al., 2019).

209 Since the mid-20th century, also clay mineralogy is widely used as a tracer of
210 paleoclimate (Klingebiel, 1963; Sittler and Millot, 1964; Power, 1969; Bierkland, 1969).

211 The assumption that clay assemblages reflect coeval climate conditions is supported by
212 the long known distribution of clay minerals around the world's oceans largely reflects
213 climate and weathering in adjacent continental areas (Biscaye, 1965; Griffin et al., 1968).

214 For example, kaolinite is abundant in wet areas where chemical weathering is intense,
215 smectite is common in warm regions with a well-defined dry season characterized by
216 intense evaporation, and illite and chlorite dominate where erosion is chiefly physical
217 and decomposition is minor (Chamley, 1989; Velde, 1996). A discussion on the weakness
218 of clay assemblages as proxies of weathering intensity is presented below. Other authors
219 used a Mineralogical Index of Alteration (MIA) based on the proportions of quartz and
220 feldspar (Rieu et al., 2007; Hessler et al., 2017). The proportion of these minerals,
221 however, largely depends on sediment grain-size, hampering the application of such
222 index in interpretations of climate-driven weathering (Garzanti et al., this volume).

224 3. The Congo and southwest Africa case-study

226 Southwest Africa has excellent conditions to review the links between sediment
227 composition, weathering intensity and climate. This vast region is characterized by a
228 stark contrast in climatic conditions (Fig. 1), and also the other factors that affect mud

composition are spatially variable, namely physiography (e.g., slope, size of drainage basins, elevation of flat and step areas, relation between topography and climatic variables) and geology (e.g., crystalline rocks of different composition, lava fields, proportion of multicycle sedimentary successions) (Fig. 2; Appendix A).

233

234 3.1. Geology and geomorphology

235 3.1.1. Atlantic margin

Several Cretaceous and Cenozoic stages of uplift affected the western margin of southern Africa after initial opening of the South Atlantic (Burke and Gunnell, 2008; Guillocheau et al., 2018). These tectonic processes, which controlled the development of Meso-Cenozoic sedimentary basins and the configuration of the drainage network, are most prominent in southern locations where more than 4000 m of crustal uplift is estimated (Jackson et al., 2005; Guiraud et al., 2010). Along the Atlantic margin of the Democratic Republic of Congo (DRC) and Angola, an Upper Cretaceous to Holocene sedimentary succession reaching several km in thickness is widely exposed in onshore areas of the Lower Congo (~85 km), Kwanza (~ 135 km), and Namibe (~50 km) basins (e.g., Moulin et al., 2010; Chaboureau et al., 2013 and references herein). The succession starts with coarse-grained siliciclastic deposits followed by thick evaporites overlain by siliciclastic and carbonate units deposited in marine and coastal continental environments (Guiraud et al., 2010). This continental margin is mainly volcanic-poor (Contrucci et al., 2004; Séranne and Anka, 2005), although Lower Cretaceous syn-rift mafic volcanic rocks occur (Marzoli et al., 1999).

251 The basement includes Archean rocks of the Congo craton and bordering Proterozoic
 252 orogenic belts associated with the amalgamation of West Gondwana (Basei et al., 2008;
 253 Heilborn et al., 2008; Vaughan and Pankhurst, 2008). In northern locations, Meso-
 254 Cenozoic strata non-conformably overlie Paleoproterozoic crystalline units that define a
 255 < 100 km-wide elongated ribbon to the west of the Neoproterozoic West Congo Belt.
 256 The latter includes mid-Paleoproterozoic (~2 Ga) basement and Tonian metamorphic
 257 and volcano-sedimentary rocks with eastward-decreasing deformation and
 258 metamorphic grade, covered by Cryogenian to Ediacaran siliciclastic and carbonate
 259 strata (Tack et al., 2001; Kadima et al., 2011). Basement geology changes south of ~10°
 260 S, where the Congo craton is mostly represented by Eburnean (~2 Ga) granitoids of the
 261 Angola Block (de Waele et al., 2008). The Angola Block also includes Neoarchean
 262 granitoids, high-grade metamorphic rocks, and mafic complexes at its north-eastern
 263 edge (Carvalho et al., 2000), and large mafic intrusions of the Mesoproterozoic Cunene
 264 Intrusive Complex at its south-eastern edge (Carvalho et al., 2000; Mayer et al., 2004;
 265 Becker et al., 2006). A poli-orogenic complex with reworked Precambrian crystalline
 266 rocks is exposed to the west and reaches ~150 km in width in southern sectors.
 267 More than 200 km from the coastline, occurs a mainly Cenozoic, sand-dominated fluvial
 268 and aeolian succession of the Kalahari Basin (Wiggs et al., 1995; Haddon and McCarthy,
 269 2005). The Kalahari succession is preserved in a relatively continuous subsiding area
 270 between the Republic of South Africa and the DRC, although with discrete depocenters
 271 that started to form during the Late Cretaceous or Early Cenozoic following uplift of
 272 southern African margins (Haddon and McCarthy, 2005).

709
710
711 274 3.1.2. Congo river basin
712

713
714 275 With a catchment area of approximately 3.7 million km² and 4200 km-long, the Congo
715
716 276 is one of the largest rivers in the world, draining most of the DRC as well as significant
717
718 277 portions of the Central African Republic, Angola, Zambia, Cameroon, and Tanzania. In
719
720
721 278 central position, a broadly circular intra-cratonic basin 1000-1300 km in diameter
722
723 279 (Congo Basin or *Cuvette Centrale*) coincides with a pronounced negative long-
724
725 280 wavelength gravimetric anomaly (Crosby et al., 2010). The Congo Basin is an old
726
727
728 281 subsiding continental area bounded by topographic highs that started to develop during
729
730 282 the Late Proterozoic, probably in relation with failed-rift processes, and presents an up
731
732 283 to 9 km-thick sedimentary fill ranging in age from the late Neoproterozoic to the
733
734 284 Holocene (Daily et al., 1992; Kadima et al., 2011).

735
736
737 285 The Congo Basin fill, thicker in a central area dominated by Cenozoic sediments,
738
739 286 becomes thinner towards the margins where older units are exposed; Jurassic to upper
740
741
742 287 Paleozoic outcrops only occur along its eastern flank (Daily et al., 1992; Giresse, 2005;
743
744 288 Fernández et al., 2015). Five major sequences were identified by Daly et al. (1992), whilst
745
746 289 Kadima et al. (2011) considered three major seismo-stratigraphic units separated by
747
748 290 basin-wide unconformities related to the Pan-African orogeny and to Permo-Triassic
749
750
751 291 deformation. Meso-Cenozoic strata, making sequence 5 of Daly et al. (1992) and seismo-
752
753 292 stratigraphic unit C of Kadima et al. (2011), crop out in wide areas of the Congo Basin.
754
755 293 The Cenozoic is well represented in the southern sector by Paleogene-Neogene deposits
756
757 294 of the Khalahari Supergroup and by Plio-Pleistocene alluvial units in the basin centre
758
759
760 295 (Fernandez-Alonso et al., 2015). These sediments were deposited when the borders of
761
762 296 the *Cuvette Centrale* were uplifted, hampering marine incursions (Giresse, 2005).
763
764
765
766
767

297 Cretaceous outcrops are most extensive along its southern edge, but occur also in
 298 numerous valleys along its eastern and northern margins. These sedimentary units were
 299 mainly deposited in continental environments by fluvial, lacustrine, or aeolian
 300 processes. Upper Jurassic and Upper Triassic strata are exposed along the banks of the
 301 Congo River and its tributaries in the eastern part of the basin (Fernandez-Alonso et al.,
 302 2015). Although Jurassic-Cretaceous strata are mainly continental, occasional marine
 303 incursions coming from the north cannot be ruled out (Giresse, 2005). Older middle to
 304 upper Paleozoic redbeds, black shales, diamictites, along with other mudstones and
 305 sandstone-dominated intervals (seismo-stratigraphic unit B of Kadima et al, 2011;
 306 sequences 3 and 4 of Daly et al, 1992) are common at the eastern edge of the basin.

307 The oldest seismo-stratigraphic unit, Neoproterozoic to early Paleozoic in age
 308 (sequences 1 and 2 of Daly et al., 1992) are exposed in three major bordering regions of
 309 the Congo Basin, making the West Congolian Group (which integrates the West Congo
 310 Super Group) along the western margin of the basin, the Lindi Supergroup to the N and
 311 NE, and the Katanga Supergroup to the SE (Fig. 2). They consist of diverse siliciclastic and
 312 carbonate rocks, including stromatolitic and evaporitic sequences deposited in marine
 313 to lagoonal environments, followed by clastic deposits (Daly et al, 1992; Kadima et al.,
 314 2011). The Precambrian basement crops out in the elevated massifs that surround the
 315 Congo Basin. Archean cratonic cores are found in the Chailu-Gabon block to the west, in
 316 the Kasai block to the south, in the North-East Congo block to the NE, and in the Tanzania
 317 craton to the east. The West Congo and Katangan/Zambezi (or Lufilian) orogenic
 318 accretionary belts at the western and south-eastern margin of the Congo Basin, were
 319 formed during the Pan-African orogeny by the deformation of Neoproterozoic and older
 320 basement units.

321

322 3.2. Climate in SW Africa

323 A pronounced climatic gradient is marked by a continuous increase in rainfall from
324 hyperarid Namibia and southern Angola to hyperhumid Congo. An oceanward decrease
325 in humidity, usually restricted to the westernmost 200-300 km of the Atlantic margin, is
326 recognised south of 2°S, whereas to the north high rainfall occurs in coastal areas (Fig.
327 1B). Unlike rainfall, average annual temperatures do not vary significantly, ranging
328 between 20 and 30°C. Lower average temperatures occur only in the most elevated
329 highlands near the eastern and southern borders of the Congo drainage basin and in
330 Angolan coastal mountains. Given these patterns of variation of rainfall and
331 temperature, climate is equatorial at lower latitudes, ranging from desert near the
332 coastline to humid subtropical or temperate-highland tropical with dry winters in inner
333 locations of higher latitudes (Peel et al., 2007).

334 Extending in latitude between approximately 9° N and 14° N, the Congo drainage basin
335 is almost entirely situated in the subequatorial zone of high rainfall and temperature.
336 Hence, with the exception of some eastern and southern marginal areas, annual rainfall
337 is invariably higher than 1000 mm and reaches more than 2000 mm in wide lower-
338 latitude sectors. The warm Angola Current explains the higher coastal humidity in
339 equatorial and sub-equatorial areas, contrasting with southern coastal regions where
340 aridity is linked with the Benguela upwelling system (Gordon and Bosley, 1991;
341 Wacongne and Piton, 1992; Stramma and Schott, 1999). The intensity of the two
342 currents and the position of their convergence zone are seasonally variable (Shannon
343 and Nelson, 1996; Kostianoy and Lutjeharms, 1999; Hardman-Mountford et al., 2003).

344 With the exception of the year-round humid equatorial region and the dry coastal fringe
345 to the south, regional climate is usually characterized by alternating wet and dry seasons
346 varying with latitude and distance from the coastline. This seasonal variability reflects
347 changes in radiation, and atmospheric and oceanic circulation patterns.

348

349 4. Methods

350 Twenty catchment areas from southwestern Africa with diverse drainage geology and
351 climate were selected for this study (Table 2). A Digital Elevation Model (DEM) based on
352 a Shuttle Radar Topography Mission (SRTM; 1 arc-second spatial resolution) was applied
353 to perform the delimitation of the catchment areas that drain to the sampling points
354 using the Hydrology tool package of ArcGIS 10. ArcGIS tools were also adopted for the
355 quantification of the outcrop areas of the main geological units in each drainage basin
356 and for the analysis of the spatial distribution of temperature and rainfall. Climatic
357 variables were downloaded from WorldClim version 2 (<http://www.worldclim.org/>; Fick
358 and Hijmans, 2017).

359 Twenty-two river mud samples, one for each catchment area, except for the Congo River
360 with three samples collected in the lower Congo course, were investigated in more
361 detail. The geochemical composition of these samples was determined for the grain-size
362 fractions $<32\ \mu\text{m}$ and $<2\ \mu\text{m}$, obtained from split aliquots by wet sieving and by
363 centrifugation according to Stokes' law, respectively. Major oxides were determined by
364 ICP-AES, using a Spectro Ciros/Arcos equipment, and trace elements by ICP-MS, using
365 an ICPMS ELAN 9000 equipment) at Bureau Veritas laboratories (Vancouver). For further
366 information on adopted procedures, geostandards used and precision see

367 <http://acmelab.com> (group 4A-4B and code LF202). The mineralogy of the <2 µm
368 fraction was determined by X-ray powder-diffraction (XRD) on oriented mounts, using a
369 Philips® PW 3710 equipment with CuKα radiation. Mineral proportions were evaluated
370 semi-quantitatively from diagnostic XRD peak areas (Moore and Reynolds, 1997; Kahle
371 et al., 2002), weighted by empirical factors (Schultz, 1964).

372 Muds collected offshore of the Congo river mouth during the Meteor cruises M6-6
373 (Wefer et al., 1988) and M20-2 (Schulz et al., 1992) were also investigated. For these
374 samples, the sand fraction (> 63 µm) was removed via wet sieving and then the clay
375 fraction (<5 µm) was separated by settling velocity, using Atterberg separation after
376 Stokes' Law (Köhn, 1928). The elemental composition of each fraction was measured
377 using a PANalytical Epsilon3-XL XRF spectrometer equipped with a rhodium tube,
378 several filters and a SSD5 detector. A calibration based on certified standard materials
379 (GBW07309, GBW07316, MAG-1) was applied to quantify elemental counts (c.f. Govin
380 et al. 2014).

381 This dataset complements previously published results on mud composition of southern
382 Africa. Namely for the clay mineralogy and the geochemistry of the <32µm fraction of
383 SW African rivers (Garzanti et al., 2014; Dinis et al., 2017); for the clay mineralogy and
384 the geochemistry of the <63µm fraction of upper Congo rivers (Garzanti et al., 2013); and
385 for the clay mineralogy of marine muds (Petschick et al., 1996).

386

387 5. Exogenous processes and mud composition

388

1004
1005
1006 389 5.1. Levels of depletion and enrichment in different grain-size fractions
1007

1008
1009 390 Significant depletions relative to the UCC are usually observed for Na, Ca, Mg, Si and K
1010
1011 391 in the fractions <2 µm and <32 µm. Only a few muds collected in small rivers of the
1012
1013 392 higher-latitude Atlantic margin show K₂O content in the coarser fraction comparable or
1014
1015 393 slightly higher than the UCC. The fraction <32 µm is invariably enriched in TiO₂ and Eu
1016
1017 394 relative to the UCC. The other elements can be either depleted or enriched in both
1018
1019 395 fractions (Fig. 3). Intersample variability is particularly high for the elements most
1020
1021 396 depleted relative to the UCC (Na and Ca), but significant variability is observed also for
1022
1023 397 a few elements that are frequently enriched relative to the UCC (e.g., light REE, Nb).
1024
1025 398 Silica, Al₂O₃ and TiO₂ display the lowest variability.
1026
1027
1028
1029

1030 399 Considering intrasample variability, the <2 µm fraction tends to be enriched in Al, Fe,
1031
1032 400 Rb, Sc and V, and strongly depleted in Zr, Hf, Na and Ca relative to the <32 µm fraction.
1033
1034 401 (Fig. 3A). The Mucope sample, which is entirely fed by recycled sediments from the
1035
1036 402 Kalahari Basin, is a notable exception yielding higher Na and Ca and lower Rb in the <2
1037
1038 403 µm fraction. The concentration of other elements can be higher in either fraction, being
1039
1040 404 usually approximately the same for Mg, REE, Y, and Nb. The concentrations of Si and Ti
1041
1042 405 also tend to be higher in the <32 µm fraction.
1043
1044
1045

1046 406 Principal Component Analysis applied to a selection of geochemical parameters
1047
1048 407 revealed that weathering plays a major role on sediment composition. River muds from
1049
1050 408 higher latitudes, where weathering is expected to be less intense, tend to plot along the
1051
1052 409 first component axis, to the left for the <32 µm fraction (Fig. 4A) and to the right for the
1053
1054 410 <2 µm fraction (Fig. 4B). The map for the <32 µm fraction shows the influence of
1055
1056 411 weathering and provenance as two perpendicular links. Weathering effects is
1057
1058
1059
1060
1061
1062

demonstrated by the correlation of the more mobile elements (Na and Ca), anti-correlated with non-mobile elements (e.g., Al_2O_3 and TiO_2). The effect of source-rock lithology is revealed by a positive correlation among MgO, MnO, and Co, anti-correlated with Th, U, W, LREE, among others that are most common in felsic rocks. These two trends are absent in the <2 fraction μm . This may reflect the fact that provenance is less important in this size fraction and the composition is almost exclusively dependent on chemical decomposition. If all the dispersion is caused by weathering much of the structure in the data would be removed. In order to better compare the levels of depletion or enrichment in different elements in the two fractions, a concentration factor α_E^{Al} (see section 2.2) was calculated for all elements. A ratio close to 1 means that the concentration of element E relative to non-mobile Al is comparable to that of the UCC. Substantially higher values indicate depletion, which can be attributed to weathering; lower values indicate enrichment. As a direct consequence of phyllosilicate concentration in finer fractions, the Al/Si ratio notoriously reflects grain-size. Thus, the values of α_E^{Al} measured for most mobile elements tend to be higher in the <2 μm fraction, where Al-rich clay minerals are concentrated. Non-mobile elements such as Sc, Y, REE, Ti, Nb tend to be relatively enriched during weathering and hence frequently show α_E^{Al} values <1. As already shown elsewhere (Dupré et al., 1996; Gaillardet et al., 1999; Viers et al., 2009; Garzanti et al., 2013, 2014), Na is the most mobile element. For the <2 μm fraction, Na ($6.8 < \alpha_{\text{Na}}^{\text{Al}} < 201$) is far more depleted than all other mobile elements, namely Ca ($3.0 < \alpha_{\text{Ca}}^{\text{Al}} < 22$), Sr ($1.8 < \alpha_{\text{Sr}}^{\text{Al}} < 19$), Mn ($0.9 < \alpha_{\text{Ca}}^{\text{Al}} < 16$), K ($1.6 < \alpha_{\text{K}}^{\text{Al}} < 5.7$) and Mg ($1.4 < \alpha_{\text{Mg}}^{\text{Al}} < 5.4$). In muds, Th, U, LREE and Fe are the most enriched elements relative to the UCC. TiO_2 , HREE, Y and Nb also tend to yield α_E^{Al} values <1 in the <32 μm fraction.

436 The high variability in concentration factors determined for some of the most mobile
 437 elements, such as Na and Ca, can be interpreted as evidence of strong weathering
 438 influence (Viers et al., 2009). The positive correlation between α_E^{Al} values in the two
 439 size-fractions is expected, whereas the poor correlation among elements such as Ti, Zr,
 440 Hf and Y hosted preferentially in the densest heavy minerals (Fig. 5B) is largely attributed
 441 to hydraulic-sorting processes. The influence of provenance coupled with hydraulic
 442 sorting is particularly evident for Zr (Fig. 5C). Factors α_{Zr}^{Al} in the two fractions of fluvial
 443 muds sampled in higher-latitude regions are similar, whereas in mid-latitude regions the
 444 levels of depletion are notably lower for the <32 μm fraction. This may be ascribed to
 445 the presence of zircon grains sourced from the felsic-rich Eburnean massifs.

446 The geochemistry of marine sediments seems to be affected by sorting processes even
 447 more than river muds. The <5 μm fraction displays a clear decrease in the Al/Si ratio and
 448 in Ti and Zr contents with water depth (Fig. 6). Lower Al content in deeper-water
 449 locations is reflected in a trend for decreasing levels of depletion in mobile elements.
 450 Precipitation of authigenic minerals (e.g., glauconite and carbonates) may have an
 451 additional effect on the levels of depletion/enrichment of different elements. Moreover,
 452 in marine realms far from fluvial entry points and in deeper marine locations the mixing
 453 of sediments transported from distant areas may overprint and blur the climatic signal
 454 hold by muds sourced from adjacent continental areas, as observed for sands offshore
 455 of the Congo mouth (Garzanti et al., this volume).

5.2. Clay mineralogy evidence of weathering

458 The clay mineralogy of most river muds considered here was presented in previous
 459 works (Garzanti et al., 2013, 2014; Dinis et al., 2017). Six new samples from the Congo
 460 River basin yield mostly kaolinite with minor amounts of mica-illite. Two new samples
 461 from the Cunene River basin are enriched in smectite and yield subordinate amounts of
 462 kaolinite, quartz, and mica. The entire dataset (Fig. 7) confirms the trends for decreasing
 463 kaolinite with latitude, which reflects a decrease in humidity and weathering intensity
 464 (Chamley, 1989; Velde, 1995). Expansive clays (smectite and smectite-illite mixed layers)
 465 are more abundant at middle and high latitudes, where seasonally contrasted climatic
 466 conditions characterized by a dry period of intense evaporation generally occurs, in
 467 particular where mafic rocks are exposed in catchment areas. Relatively high mica-illite
 468 contents in some river muds is attributed to the combined effects of earlier feldspar
 469 weathering and disintegration of micaceous minerals (Dinis et al., 2017).

470 Offshore sediments of the southeastern Atlantic are kaolinite-rich at equatorial sectors,
 471 yielding higher smectite at middle latitudes (~10-20°), and illite at farther higher
 472 latitudes (Petschick et al., 1996). In general, the ratio between kaolinite and
 473 mica+chlorite of marine samples from SW Africa is similar to river muds collected at
 474 comparable latitude (Fig. 7A), suggesting major control by river supply from adjacent
 475 continental areas. Smectite content, however, tends to increase with water depth. This
 476 is particularly evident for sediments collected offshore of the Congo River mouth, but it
 477 is also apparent in higher-latitude regions (Fig. 7B and 7C). Selective settling of kaolinite
 478 illite and chlorite, all generally coarser than smectite (Gibbs, 1977; Chamley, 1989;
 479 Petschick et al., 1996; Šimkevičius et al., 2003) may account for this basinward trend of
 480 smectite enrichment, which is not observed only at mid-latitude where fluvial and
 481 coastal muds are smectite-rich. As for sediment geochemistry, it must be kept in mind

that also the clay assemblage is affected by mixing with material transported by wind and surface or deep currents from distant sources (Petschick et al., 1996).

6. Weathering indices as climatic proxies

6.1. Relation between weathering intensity and climatic variables

Several compositional features of marine sediments, such as their clay-mineral assemblages (Biscaye, 1965; Griffin et al., 1968; Petschick et al., 1996) and element ratios (Govin et al., 2012), point to a close link with climatic conditions on adjacent continental areas. The possible links between compositional features of present-day fluvial muds and climatic variables were tested by several authors. In suspended loads of north American rivers, the concentration of non-mobile element Al and Fe correlates with runoff and precipitation, whereas an opposite trend was found for Ca and Mg (Canfield, 1997). Other works showed correlation between climatic (or climatic-driven) variables and weathering indices. Namely, between temperature and α_{Na} or α_K for big world rivers (Gaillardet et al., 1999), between runoff and CIA for Southeast Asia (Borges et al., 2008), and between rainfall and α_{Na}^{Al} in sands, α_{Mg}^{Al} in muds and clay-mineral assemblages in SW Africa rivers (Dinis et al., 2017). These relations are ascribed to higher weathering intensity in wetter settings, with consequent leaching of most mobile elements and concentration of non-mobile elements in the weathering residue. However, the scatter attributed to the effect of different geologic and geomorphologic features of the drainage areas on sediment composition is very high. Such scattering is not surprising first of all because source lithology influences both the composition of

weathering products (e.g., von Eynatten et al., 2012, 2016; Garzanti and Resentini, 2016)
 and the velocity of weathering reactions (e.g., Meybeck, 1987; Kump et al., 2000;
 Amiotte Suchez et al., 2003; Jansen et al., 2010). Despite numerous geological and
 geomorphological factors that control sediment composition, a time-scale problem may
 be also present, because a specific weathering stage may be reached after many
 thousands of years, whereas the climatic record, in terms of measured average
 temperature and rainfall, refers to the present day only and may have been notably
 different in the past.

The compositional results for mud deposits presented for the first time here can be
 coupled with the comparable datasets presented in Garzanti et al. (2013, 2014) and Dinis
 et al (2017) to better understand the relation between weathering intensity and climatic
 properties in southern Africa. Besides the equatorial and sub-tropical Atlantic margin
 and Congo system presented here in more detail, this sample set also includes muds
 from the upper branches of the Congo in DRC, Burundi, Rwanda, and Tanzania, from the
 Zambezi, Limpopo, Okavango and Orange fluvial systems, and from western Namibian
 rivers. Climate data provided by WorldClim version 2 (<http://www.worldclim.org/>; Fick
 and Hijmans, 2017) for SW Africa indicate that both rainfall and temperature display
 major spatial variability (Fig. 1). Considering average values for the catchments under
 investigation in Congo and SW Africa, rainfall is clearly more variable than temperature
 (Table 1). Furthermore, the study region is never as cold as in the case studies where the
 weathering dependence on temperature following the Arrhenius law seems to be
 applicable (e.g., White and Blum, 1991). Probably reflecting the homogenously warmer
 conditions, no significant relations were detected between temperature and any
 compositional feature indicative of weathering intensity.

Conversely, spatially-averaged rainfall co-varies with several compositional features indicative of weathering intensity (Figs. 8 and 9). Considering only geochemical parameters obtained for the <32 μm fraction (51 samples; upper Congo muds not included because the analyses were performed on the <63 μm fraction), $\alpha_{\text{Mg}}^{\text{Al}}$ ($r=0.70$), $\alpha_{\text{Ca}}^{\text{Al}}$ ($r=0.59$), WIP ($r=-0.58$), CIA ($r=0.56$), $\alpha_{\text{Sr}}^{\text{Al}}$ ($r=0.55$), and CIX ($r=0.54$) reveal the most significant correlations with rainfall. It must be noted that these correlations are weaker, or even lost, if specific climatic and geographic contexts are analysed separately (Fig. 8). As far as non-mobile elements are concerned, no significant correlation was observed within the entire dataset, but if only the Congo and the Angolan Atlantic margin are considered, $\alpha_{\text{E}}^{\text{Al}}$ for some of these elements anti-correlate with rainfall ($r=-0.73$ for Ti; $r=-0.65$ for Zr). A reasonable positive correlation between the kaolinite proportion in the clay-mineral assemblage and rainfall is also observed for the entire equatorial to sub-tropical dataset ($r=0.63$ for 66 samples).

Regarding the geochemistry of the <2 μm fraction, original data presented here indicate that average rainfall in the catchment area correlates positively with $\alpha_{\text{Mg}}^{\text{Al}}$ ($r=0.69$), CIA ($r=0.61$), $\alpha_{\text{Sr}}^{\text{Al}}$ ($r=0.58$) and $\alpha_{\text{Si}}^{\text{Al}}$ ($r=0.58$). Because of quartz dominance in the wettest settings, the link between rainfall and the WIP is much weaker than in the <32 μm fraction, and the weakest among all of the other multi-element weathering indices. The highest negative correlation is found for $\alpha_{\text{Cs}}^{\text{Al}}$ ($r=-0.57$).

6.2. Spurious covariance of compositional features and rainfall

As shown by Garzanti and Resentini (2016), the values obtained for weathering indices may be largely determined by source-area lithology. In southern Africa, some co-

variances between measured element abundances and rainfall are in fact influenced by geological and geomorphological features independent of climate. One evident case is the abundance of Ca and other mobile elements incorporated in carbonate minerals, which is expected to be higher where carbonate rocks are exposed. High Ca, Mg, and Sr actually occur in coarser mud fractions from southern rivers characterized by moderately dry to very dry conditions that drain Meso-Cenozoic basins of the Atlantic Margin or from hinterland areas prone to pedogenic carbonate precipitation within the Kunene and Okavango river systems (Caculuar and Kwando rmuds). Sorting processes also seem to have a major effect on the abundances of non-mobile elements in coarser mud fractions, as suggested before for Zr and Ti, among other elements that tend to concentrate in heavy minerals (Fig. 5). Hence, provenance and sorting processes can play a major role on mud composition, in particular if silt particles are present, leading to spurious correlations with rainfall. They may have forged apparent relations between the concentration of mobile/non-mobile elements and rainfall that are not necessarily linked with present-day climatically-driven chemical weathering.

6.3 Focus on the clay fraction

Sediment composition is strongly influenced by grain-size (von Eynatten et al., 2012, 2016). Because mud deposits may integrate different proportions of clay and silt, even an analysis focused on mud may lead to biased interpretations of climate conditions. A closer relationship between clay mineralogy and chemical weathering than that observed for the geochemistry of muds comprising coarser silt fractions was already shown for the Angolan Atlantic margin (Dinis et al., 2017). In that research, however,

the geochemistry of clay was not investigated, and X-ray Diffraction (XRD) is unable to provide accurate quantitative assessments of mineral abundances (Moore and Reynolds, 1997; Kahle et al., 2002). For instance, a mixture in equal proportions of kaolinite, smectite and chlorite, three minerals indicating profoundly distinct climatic conditions, shows unequal (001) peak areas that depend on the chemical compositions, preferred orientation, and structural arrangement of clay flakes.

More accurate results are expected from geochemical data. Classical multi-elements weathering indices (e.g., CIA, WIP, CIX and CPA) and the α_E and α_E^{Al} indices used to establish element mobility are computed from ratios of the concentration of one or more mobile elements relative to non-mobile references; WIP consider the abundance of a set on mobile element. The concentrations of the mobile and non-mobile elements considered in these parameters vary not just with grain-size, but also with the mineralogy of the source rock, being the differences between sediments generated from felsic and mafic source rocks usually attenuated in the finer fractions (von Eynatten et al., 2012, 2016; Dinis et al., 2017). The readily leaching of mobile elements in finer fractions with formation of residues enriched in Al regardless of source rock composition partially accounts for this attenuation trend. In addition, silt particles are still strongly influenced by hydraulic-sorting process, as shown by the scattering of the levels of depletion/enrichment discussed before (Fig. 5). Clay fractions are not equally influenced by sorting processes, and therefore more likely to reflect weathering processes coeval with deposition (Guo et al., 2018). Given the minor influence of hydraulic fractionation on clay geochemistry, the originally defined mobility indices α of Gaillardet et al. (1999) may not be distorted by these processes as much as when applied to sediments made of coarser silt and sand particles.

Not all geochemical parameters from the clay fraction are as robust as estimators of climatic variables. For instance, K abundance in clay may be strongly dependent on source-area geology (von Eynatten et al., 2012, 2016), and indices including K such as CIA, WIP, CIX, α_K^{Th} , or α_K^{Al} may consequently not be faithful proxies of rainfall. Other indices (e.g., CPA, α_{Na}^{Al} and α_{Na}^{Sm}) rely on Na as the mobile element, which however is generally quite scarce in the clay-mineral lattice. In SW African river muds, Na_2O concentrations are locally near the detection level of 0.01%, hence introducing a supplementary risk of biased interpretation. Magnesium does not suffer from these issues, because it is invariably present in significant amounts in clay and, despite overt differences between the fine-grained fractions produced from mafic and felsic rocks in cold settings (Louvat et al., 2008; von Eynatten et al., 2012), the divergence seems to be reduced as weathering progresses, being apparently minor in clays produced under wet and warm settings (von Eynatten et al., 2016). This is confirmed by the fact that in our study α_{Mg}^{Al} resulted to be a slightly better estimator of rainfall than other compositional parameters (Fig. 9).

6.4. Geological and geomorphological causes of scatter

This section is dedicated to a selection of factors that are likely to affect the composition of the finer-grained component of mud deposits. Other causes of dispersion, such as the mafic vs. felsic character of source rocks and heterogeneities in grain-size distribution, which should have higher influence on the composition of coarser sediment fractions, have been discussed above.

1594
1595
1596 622 6.4.1. Supply from areas with different climate
1597

1598
1599 623 While evaluating weathering in the source area of sediments, we must keep in mind that
1600
1601 624 chemical processes generally do not take place in homogenous environmental
1602
1603 625 conditions. In big drainage basins transitory deposition must limit the influence of the
1604
1605 626 processes taking place in the most distant sectors of the basin of the basin on the
1606
1607 627 composition of sediments relative to more proximal sites. Sediment composition can be
1608
1609 628 affected also by processes occurring outside the drainage basins, as observed within or
1610
1611 629 close to arid and semiarid regions, where a significant fraction of fine-grained deposits
1612
1613 630 seems to be allochthonous and airborne, formed in regions of completely different
1614
1615 631 climate rather than generated in the river basin itself. Significant amounts of far-
1616
1617 632 travelled sands was recognised in SW Africa (Garzanti et al., 2018a, 2018b) and this is
1618
1619 633 even more plausible for very fine-grained particles. A similar complication has been
1620
1621 634 discussed for marine deposits above.
1622
1623
1624
1625
1626

1627 635

1628
1629
1630 636 6.4.2. Recycling
1631

1632 637 Even if only sediments produced within the drainage basin are considered, a major and
1633
1634 638 long-recognised problem is the possible inheritance of compositional features from
1635
1636 639 older sedimentary rocks (e.g., Borges et al., 2008; Garzanti and Resentini, 2016).
1637
1638 640 Therefore, weathering indices generally reflect chemical processes cumulated during
1639
1640 641 multiple depositional cycles, rather than weathering-related transformations coeval
1641
1642 642 with the depositional unit. This problem is particularly pertinent in large catchment
1643
1644 643 areas such as that of the Congo River, that include wide exposures of units formed in
1645
1646 644 diverse previous sedimentary cycles (Gaillardet et al., 1999). Although different methods
1647
1648
1649
1650
1651
1652

1653
1654
1655 645 were proposed to address the effect of recycling on weathering indices (Gaillardet et al.,
1656 646 1999; Garzanti et al., 2013; Dinis et al., 2017), it remains an issue difficult to solve.
1657 647 Comparing the composition of daughter sediments and parent rocks is a plausible way
1658 648 to quantitatively assess weathering-driven transformations during the last depositional
1659 649 cycle (Chetelat et al., 2015; Dinis and Oliveira, 2016). However, it may be quite difficult
1660 650 to accurately evaluate average source-rock composition in large catchment areas.

1661
1662 651 Whereas sand is largely the product of physical erosion, clay-rich muds are chiefly the
1663 652 product of climatically-driven weathering, which explains their stronger depletion in
1664 653 mobile elements. However, sand may also show extreme depletion in mobile elements
1665 654 whenever the effect of chemical processes during weathering and recycling is cumulated
1666 655 through multiple sedimentary cycles. A long multicyclic history typically ends up in
1667 656 quartz-enrichment (Garzanti, 2017), which is the case of Congo River sand that only
1668 657 includes the most chemically durable minerals (Garzanti et al., this volume). Congo
1669 658 muds, however, yield relatively low silica (34-43% in the <2 µm fraction), which is
1670 659 leached in association to kaolinite formation, and are enriched in some the of the least
1671 660 mobile elements (i.e., Al and Ti). When weathering is not extreme, as in the intra-
1672 661 cratonic Kalahari Basin where quartz is present in the clay fraction, recycling may
1673 662 promote silica enrichment in river muds (up to 58% SiO₂ in the <2 µm fraction and up to
1674 663 66% in the <32 µm fraction). Recycling thus affects the composition of coarse and fine
1675 664 particles differently.

1676 665 Silt and clay particles in fluvial mud deposits are entrained in suspension and tend to
1677 666 concentrate at different channel depths during transport. Finest-grained particles occur
1678 667 preferentially at shallower depths (Rouse, 1937; Vanoni, 2006). They are kept in motion

even when current velocity and competence decrease in the lowlands, being more likely
 winnowed offshore in hypopycnal plumes. Finest particles are also the most easily
 transported by wind. Based on these considerations, we hypothesize that the amount
 of this finest component is preferentially lost during multiple sedimentary cycles. If this
 is true, then this finest component would represent climatic conditions during the last
 cycle better than coarser fractions, and the ratio of the same weathering index in
 different grain-size fractions (e.g., $<2\ \mu\text{m}$ vs. $<32\ \mu\text{m}$) may be used to assess recycling
 effects. This possibility is supported by the covariance of this ratio calculated for the
 level of depletion of a most mobile element (i.e., ratio of $\alpha_{\text{Na}}^{\text{Al}}$ in the $<2\ \mu\text{m}$ vs. $<32\ \mu\text{m}$
 fractions) with the percentage of Meso-Cenozoic sedimentary units in respective source
 areas (Fig. 10). River muds with similar levels of Na-depletion in the two size fractions
 that does not follow this trend were sampled either in arid to semi-arid settings where
 airborne particles are most likely present, or in catchment areas including sedimentary
 rocks of the West Congo Belt. In both cases, sources of recycled material alternative to
 Meso-Cenozoic sedimentary successions occur. As for other parameters, however, the
 influence of grain-size and source-area geology on coarser mud fractions and the very
 low Na contents in the clay fraction when weathering is intense limits the application of
 this ratio as an estimator of recycling component.

6.4.3. Influence of geomorphological features on weathering processes

The size and relief of the catchment also exert a significant influence on sediment
 composition (e.g., Weaver, 1989). In small and relatively steep catchments,
 heterogeneities in the exposed lithological units are not averaged out and sediment

1771
1772
1773
1774
1775
1776
1777
1778
1779
1780
1781
1782
1783
1784
1785
1786
1787
1788
1789
1790
1791
1792
1793
1794
1795
1796
1797
1798
1799
1800
1801
1802
1803
1804
1805
1806
1807
1808
1809
1810
1811
1812
1813
1814
1815
1816
1817
1818
1819
1820
1821
1822
1823
1824
1825
1826
1827
1828
1829

691 composition is expected to mirror the composition of those source rocks that erode
692 faster. In steep areas, chemical decomposition is frequently hampered by the rapidity
693 of erosion processes (weathering-limited regimes of Riebe et al., 2004, and West et al,
694 2005) and weathering reactions should be particularly incomplete. Conversely, because
695 widely different climatic conditions are generally present in large rivers, the relationship
696 between sediment composition and climatic parameters is more complex. In addition,
697 sediment temporarily stored in alluvial plains can suffer additional decomposition (e.g.,
698 Johnsson and Meade, 1990). Several authors defended that floodplains are likely sites
699 of weathering reactions (Galy and France-Lanord, 1999; West et al., 2002; Moquet et
700 al., 2011), although minor changes in suspended load after transitory deposition were
701 also reported (Bouchez et al., 2012). Assessment of climatic conditions from mud
702 composition may thus be more reliable when dealing with drainage basins of medium
703 size. In the present case, if data from sediments carried by the huge Congo River and by
704 the rivers with drainage areas smaller than 2000 km² are neglected, the correlation
705 between rainfall and α_{Mg}^{Al} is in fact notably improved (Fig. 9).

706 Also to be considered is that water availability does not depend exclusively on rainfall,
707 but can be linked with the proximity of the water table. Weathering rates strongly
708 depend on fluid residence times and flow rates (Maher, 2010), and high weathering
709 intensities may be attained in more permeable mediums (Weaver, 1989; Hundert et al.,
710 2006).

711

712 6.4.4. Biogeochemical cycling

1830
1831
1832 713 Finally, the fluxes of weathering-related elements and soil composition depend on the
1833
1834 714 interactions with vegetation and nutrient cycling (Minasny et al., 2015). Magnesium,
1835
1836 715 along with other mobile elements, is an important nutrient influenced by
1837
1838 716 biogeochemical cycles (White and Bum, 1995; Rufyikiri et al., 2004; Sardans et al., 2008;
1839
1840 717 Barré et al., 2009). The transfers promoted by plants' activity are thus likely to be
1841
1842 718 responsible for changes in inorganic element concentration in the upper levels of soil
1843
1844 719 profiles, which are most promptly eroded to generate fine particles entrained as
1845
1846 720 suspended load.
1847
1848
1849
1850
1851 721
1852
1853
1854 722 7. Concluding remarks
1855
1856
1857 723
1858
1859
1860 724 Weathering intensity is largely influenced by climate, it can be estimated from the
1861
1862 725 geochemical and mineralogical composition of sediments and thus can be able to
1863
1864 726 approximate past climatic conditions. A series of problems, however, arise when
1865
1866 727 geochemical and mineralogical indices are used as climatic proxies. This is because
1867
1868 728 sediment composition is controlled by diverse factors that may overprint the effect of
1869
1870 729 climate, making paleoclimate interpretations ambiguous and uncertain. The
1871
1872 730 composition of detrital daughter sediments is controlled primarily by the composition
1873
1874 731 of the parent rocks. Moreover, even where source-rock geology is similar, sediment
1875
1876 732 composition will depend on the grain size of the generated sediments. Mineralogical
1877
1878 733 and even more drastically chemical composition of sediments may be strongly
1879
1880 734 influenced by hydraulic-sorting processes, which controls the distribution of minerals
1881
1882 735 with different density and shape in different size fractions. Other elusive factors that
1883
1884
1885
1886
1887
1888

736 may be difficult to cope with are the dependence on the geomorphology of the drainage
 737 basin (e.g., size of the catchment, variable hillslopes and yields from different basin
 738 locations, proximity of the phreatic level) and the widespread and commonly
 739 overwhelming contribution of detritus recycled from pre-existing sedimentary units.
 740 Climatic conditions are poorly reflected in the mineralogical and chemical composition
 741 of sand and coarse silt, which is largely generated by physical processes and is more
 742 affected by quartz dilution through sediment recycling. Finer-grained sediments, and
 743 especially the clay fraction, are more promising because heterogeneities in particle size
 744 tend to be lower and they are markedly enriched in material eroded from coeval soils,
 745 thus able to more faithfully reflect the environmental conditions during the last
 746 depositional cycle. In addition, it appears that the composition of clay is somewhat less
 747 dependent on the felsic vs. mafic provenance than coarser detritus. Fairly robust
 748 relationships between clay geochemistry and rainfall were in fact obtained for southern
 749 African river muds. The finer size-fraction, however, is most likely affected by several
 750 other interfering factors, such as the presence of airborne allochthonous material, as
 751 well as by the process of plant uptake of mineral nutrients (e.g., Mg, Ca, and K). Problems
 752 of analytical accuracy, such as imprecision in the quantitative estimation of XRD
 753 mineralogy and of the concentrations of the most mobile elements can also be a cause
 754 of noise. Links between mud composition and climatic properties are even more difficult
 755 to establish in the marine environment. Here, mineral segregation by grain-size, mixture
 756 with allochthonous sediment transported by air or water currents from distant
 757 continental or intraoceanic areas, and formation of authigenic minerals commonly have
 758 a major effect on the composition of the clay fraction. Furthermore, muds are

1948
1949
1950 759 particularly vulnerable to post-depositional diagenetic transformations that inevitably
1951
1952 760 blur the climatic signal in sediments deposited in any environment.
1953
1954
1955 761 Despite these difficulties, regional climatic proxies based on mud composition are not
1956
1957 762 destined for the dustbin. Mud is found in great abundance in all fluvial deposits
1958
1959 763 worldwide. Sampling mud deposits, separating their clay fraction and determining their
1960
1961 764 geochemical and mineralogical composition are simple and non-expensive tasks. The
1962
1963 765 main challenge is to isolate the role played by the number of sedimentological,
1964
1965 766 geomorphological, and biological factors that influence mud composition besides
1966
1967 767 climatically-driven weathering. This can be partially achieved with large datasets from
1968
1969 768 distinct size-fractions that are affected differently by diverse controlling factors.
1970
1971 769 Advances in these issues will improve the performance of mud composition as an
1972
1973 770 independent tool capable of approximating past climatic conditions in continental
1974
1975 771 settings.
1976
1977
1978
1979 772
1980
1981 773
1982
1983
1984 774 Acknowledgments
1985
1986
1987 775 The present work was supported by the FCT (Portuguese National Board of Scientific
1988
1989 776 Research) through the Strategic Program MARE- Marine and Environmental Sciences
1990
1991 777 Centre (UID/MAR/04292/2013).
1992
1993
1994 778
1995
1996
1997
1998 779 References
1999
2000
2001
2002
2003
2004
2005
2006

- 2007
2008
2009 780 Aitchison, J. (1986). The statistical analysis of compositional data. London, Chapman &
2010
2011 781 Hall.
2012
2013
2014 782 Aitchison, J., Greenacre, M. (2002). Biplots of compositional data. Journal of the Royal
2015
2016 783 Statistical Society: Series C (Applied Statistics) 51, 375-392.
2017
2018
2019 784 Alroy, J., Koch, P.L., Zachos, J.C. (2000). Global climate change and North American
2020
2021 785 mammalian evolution. Paleobiology 26, 259-288.
2022
2023
2024 786 Amiotte Suchet, P., Probst, J.L., Ludwig, W. (2003). Worldwide distribution of continental
2025
2026 787 rock lithology: Implications for the atmospheric/soil CO₂ uptake by continental
2027
2028 788 weathering and alkalinity river transport to the oceans. Global Biogeochemical
2029
2030 789 Cycles, 17, <https://doi.org/10.1029/2002GB001891>.
2031
2032
2033 790 Araújo, A.G. Perevalov, O.V., 1998. Carta de recursos minerais de Angola/Mineral
2034
2035 791 resources map of Angola. Ministério de Geologia e Minas, Instituto Geológico de
2036
2037 792 Angola.
2038
2039
2040 793 Babechuk, M.G., Widdowson, M., Kamber, B.S., 2014. Quantifying chemical weathering
2041
2042 794 intensity and trace element release from two contrasting basalt profiles, Deccan
2043
2044 795 Traps, India. Chemical Geology 363, 56-75.
2045
2046
2047 796 Barré, P., Berger, G., & Velde, B. (2009). How element translocation by plants may
2048
2049 797 stabilize illitic clays in the surface of temperate soils. Geoderma 151, 22-30.
2050
2051
2052 798 Basei, M.A.S., Frimmel, H.E., Nutman, A.P., Preciozzi, F., 2008. West Gondwana
2053
2054 799 amalgamation based on detrital zircon ages from Neoproterozoic Ribeira and
2055
2056 800 Dom Feliciano belts of South America and comparison with coeval sequences
2057
2058 801 from SW Africa. Geological Society, London, Special Publications, 294, 239-256.
2059
2060
2061
2062
2063
2064
2065

802 Becker, T., Schreiber, U., Kampunzu, A. B., Armstrong, R., 2006. Mesoproterozoic rocks
 803 of Namibia and their plate tectonic setting. *Journal of African Earth Sciences* 46,
 804 112-140.
 805 Bernard, A., Daux, V., Lécuyer, C., Brugal, J. P., Genty, D., Wainer, K., ... & Jaubert, J.
 806 (2009). Pleistocene seasonal temperature variations recorded in the $\delta^{18}\text{O}$ of
 807 *Bison priscus* teeth. *Earth and Planetary Science Letters* 283, 133-143.
 808 Birkeland, P. W. (1969). Quaternary paleoclimatic implications of soil clay mineral
 809 distribution in a Sierra Nevada-Great Basin transect. *The Journal of Geology* 77,
 810 289-302.
 811 Biscaye, P.E. (1965). Mineralogy and sedimentation of recent deep-sea clay in the
 812 Atlantic Ocean and adjacent seas and oceans. *Geological Society of America*
 813 *Bulletin* 76, 803-832.
 814 Borges, J.B., Huh, Y., Moon, S., Noh, H. (2008). Provenance and weathering control on
 815 river bed sediments of the eastern Tibetan Plateau and the Russian Far East.
 816 *Chemical Geology* 254, 52-72.
 817 Bouchez, J., Gaillardet, J., France-Lanord, C., Maurice, L., Dutra-Maia, P. (2011). Grain
 818 size control of river suspended sediment geochemistry: Clues from Amazon River
 819 depth profiles. *Geochemistry, Geophysics, Geosystems* 12,
 820 <https://doi.org/10.1029/2010GC003380>
 821 Bouchez, J., Gaillardet, J., Lupker, M., Louvat, P., France-Lanord, C., Maurice, L., ... &
 822 Moquet, J. S. (2012). Floodplains of large rivers: Weathering reactors or simple
 823 silos? *Chemical Geology* 332, 166-184.

- 824 Bradly, P.V. and Carrol, S.A. (1994). Direct effects of CO₂ and temperature on silicate
825 weathering: possible implications for climate control. *Geochimica and*
826 *Cosmochimica Acta* 58, 1853-1856.
- 827 Buggle, B., Glaser, B., Hambach, U., Gerasimenko, N., Markovic, S., 2011. An evaluation
828 of geochemical weathering indices in loess-paleosol studies. *Quaternary*
829 *International* 240, 12-21.
- 830 Burke, K., Gunnell, Y. (2008). The African erosion surface: a continental-scale synthesis
831 of geomorphology, tectonics, and environmental change over the past 180
832 million years (Vol. 201). Geological Society of America.
- 833 Canfield, D.E. (1997). The geochemistry of river particulates from the continental USA:
834 major elements. *Geochimica et Cosmochimica Acta* 61, 3349-3365.
- 835 Carvalho, H., Tassinari, C., Alves, P.H., Guimarães, F., Simões, M.C., 2000.
836 Geochronological review of the Precambrian in western Angola: links with Brazil.
837 *Journal of African Earth Sciences* 31, 383-402.
- 838 Chaboureaud, A.-C., Guillocheau, F., Robin, C., Rohais, S., Moulin, M., Aslanian, D., 2013.
839 Paleogeographic evolution of the central segment of the South Atlantic during
840 Early Cretaceous times: Paleotopographic and geodynamic implications.
841 *Tectonophysics* 604, 191-223.
- 842 Chetelat, B., Liu, C. Q., Wang, Q., Zhang, G. (2013). Assessing the influence of lithology
843 on weathering indices of Changjiang river sediments. *Chemical Geology* 359, 108-
844 115.

- 845 Clift, P.D., Wan, S., Blusztajn, J. (2014). Reconstructing chemical weathering, physical
846 erosion and monsoon intensity since 25 Ma in the northern South China Sea: a
847 review of competing proxies. *Earth-Science Reviews* 130, 86-102.
- 848 Contrucci, I., Matias, L., Moulin, M., Géli, L., Klingelhofer, F., Nouzé, H., Aslanian, D.,
849 Olivet, J.L., Réhault, J.P., Sibuet, J.C. (2004). Deep structure of the West African
850 continental margin (Congo, Zaïre, Angola), between 5°S and 8°S, from
851 reflection/refraction seismics and gravity data. *Geophysical Journal International*
852 158, 529-553.
- 853 Crosby, A. G., Fishwick, S., & White, N. (2010). Structure and evolution of the
854 intracratonic Congo Basin. *Geochemistry, Geophysics, Geosystems* 11,
855 <https://doi.org/10.1029/2009GC003014>
- 856 Daly, M. C., Lawrence, S. R., Diemu-Tshiband, K., Matouana, B. (1992). Tectonic
857 evolution of the Cuvette Centrale, Zaire. *Journal of the Geological Society* 149,
858 539-546.
- 859 de Waele, B., Johnson, S. P., Pisarevsky, S.A. (2008). Palaeoproterozoic to
860 Neoproterozoic growth and evolution of the eastern Congo Craton: its role in the
861 Rodinia puzzle. *Precambrian Research* 160, 127-141.
- 862 Deconinck, J.F., Hesselbo, S.P., Debuisser, N., Averbuch, O., Baudin, F., Bessa, J. (2003).
863 Environmental controls on clay mineralogy of an Early Jurassic mudrock (Blue
864 Lias Formation, southern England). *International Journal of Earth Sciences* 92,
865 255-266.

866 Dessert, C., Dupré, B., Gaillardet, J., François, L. M., Allegre, C.J. (2003). Basalt
867 weathering laws and the impact of basalt weathering on the global carbon cycle.
868 Chemical Geology 202, 257-273.

869 Diefendorf, A.F., Mueller, K.E., Wing, S.L., Koch, P.L., Freeman, K.H. (2010). Global
870 patterns in leaf ^{13}C discrimination and implications for studies of past and future
871 climate. Proceedings of the National Academy of Sciences 107, 5738-5743.

872 Dinis, P., Oliveira, Á. (2016). Provenance of Pliocene clay deposits from the Iberian
873 Atlantic Margin and compositional changes during recycling. Sedimentary
874 Geology 336, 171-182.

875 Dinis, P., Garzanti, E., Vermeesch, P., Huvi, J. (2017). Climatic zonation and weathering
876 control on sediment composition (Angola). Chemical Geology 467, 110-121.

877 Dupré, B., Dessert, C., Oliva, P., Goddérís, Y., Viers, J., François, L., Millot, R., Gaillardet,
878 J. (2003). Rivers, chemical weathering and Earth's climate. Comptes Rendus
879 Geoscience 335, 1141-1160.

880 Dupré, B., Gaillardet, J., Rousseau, D., Allègre, C.J., 1996. Major and trace elements of
881 river-borne material: The Congo Basin. Geochimica et Cosmochimica Acta, 60,
882 1301-1321.

883 Ehrmann, W. (1998). Implications of late Eocene to early Miocene clay mineral
884 assemblages in McMurdo Sound (Ross Sea, Antarctica) on paleoclimate and ice
885 dynamics. Palaeogeography, Palaeoclimatology, Palaeoecology 139, 213-231.

886 Ernst, R. E., Pereira, E., Hamilton, M. A., Pisarevsky, S. A., Rodriques, J., Tassinari, C. C.,
887 ... Van-Dunem, V. (2013). Mesoproterozoic intraplate magmatic 'barcode' record

888 of the Angola portion of the Congo Craton: Newly dated magmatic events at 1505
 889 and 1110 Ma and implications for Nuna (Columbia) supercontinent
 890 reconstructions. *Precambrian Research* 230, 103-118.
 891 Fedo, C.M., Nesbitt, H. W., Young, G.M. (1995). Unraveling the effects of potassium
 892 metasomatism in sedimentary rocks and paleosols, with implications for
 893 paleoweathering conditions and provenance. *Geology* 23, 921-924.
 894 Fernandez-Alonso, M. et al. (2015). Carte Géologique de la République Démocratique
 895 du Congo. République Démocratique du Congo, Ministère des Mines.
 896 Fick, S.E. and Hijmans, R.J., 2017. Worldclim 2: New 1-km spatial resolution climate
 897 surfaces for global land areas. *International Journal of Climatology* 37, 4302-
 898 4315.
 899 Gabet, E. J., Mudd, S. M. (2009). A theoretical model coupling chemical weathering rates
 900 with denudation rates. *Geology* 37, 151-154.
 901 Gaillardet, J., Dupré, B., Allègre, C.J. (1999). Geochemistry of large river suspended
 902 sediments: silicate weathering or recycling tracer? *Geochimica et Cosmochimica*
 903 *Acta* 63, 4037-4051.
 904 Gallet, S., Jahn, B. M., Lanoë, B. V. V., Dia, A., & Rossello, E. (1998). Loess geochemistry
 905 and its implications for particle origin and composition of the upper continental
 906 crust. *Earth and Planetary Science Letters* 156, 157-172.
 907 Galy, A., France-Lanord, C. (1999). Weathering processes in the Ganges–Brahmaputra
 908 basin and the riverine alkalinity budget. *Chemical Geology* 159, 31-60.

- 909 Galy, V., France-Lanord, C., Lartiges, B. (2008). Loading and fate of particulate organic
910 carbon from the Himalaya to the Ganga-Brahmaputra delta. *Geochimica et*
911 *Cosmochimica Acta* 72, 1767-1787.
- 912 Garrels, R.M. (1983). The carbonate-silicate geochemical cycle and its effect on
913 atmospheric carbon dioxide over the past 100 million years. *American Journal of*
914 *Science* 283, 641-683.
- 915 Garzanti E., 2017. The maturity myth in sedimentology and provenance analysis. *Journal*
916 *of Sedimentary Research*, 87, 353-365.
- 917 Garzanti, E., Andó, S., Vezzoli G., 2009. Grain-size dependence of sediment composition
918 and environmental bias in provenance studies. *Earth and Planetary Science*
919 *Letters* 277, 422-432.
- 920 Garzanti, E., Padoan, M., Setti, M., López-Galindo, A., & Villa, I. M. (2014). Provenance
921 versus weathering control on the composition of tropical river mud (southern
922 Africa). *Chemical Geology*, 366, 61-74.
- 923 Garzanti, E., Padoan, M., Setti, M., Peruta, L., Najman, Y., Villa, I.M. (2013). Weathering
924 geochemistry and Sr-Nd isotope fingerprinting of equatorial upper Nile and
925 Congo muds. *Geochemistry, Geophysics, Geosystems* 14, 292-316.
- 926 Garzanti, E., Resentini, A. (2016). Provenance control on chemical indices of weathering
927 (Taiwan river sands). *Sedimentary geology* 336, 81-95.
- 928 Garzanti, E., Dinis, P., Vermeesch, P., Andò, S., Hahn, A., Huvi, J., Limonta, M., Padoan,
929 M., Resentini, A., Rittner, M., Vezzoli, G., 2018a. Sedimentary processes

- controlling ultralong cells of littoral transport: Placer formation and termination
of the Orange sand highway in southern Angola. *Sedimentology* 65(2), 431-460.
- Garzanti, E., Dinis, P., Vermeesch, P., Andò, S., Hahn, A., Huvi, J., Limonta, M., Padoan, M., Resentini, A., Rittner, M., Vezzoli, G., 2018b. Dynamic uplift, recycling, and climate control on the petrology of passive-margin sand (Angola). *Sedimentary Geology* 375, 86-104.
- Garzanti, E., Vermeesch, P., Andó, S., Limonta, M., Vezzoli G., Dinis, P., Hahn, A., Baudet, D., de Grave, J., Yaya, N.K. (this volume). Congo river sand and the equatorial quartz factory. *Earth Sciences Reviews* (submitted to the present issue).
- Gibbs, R.J. (1977). Clay mineral segregation in the marine environment. *Journal of Sedimentary Research* 47, 237-243.
- Giresse, P. (2005). Mesozoic–Cenozoic history of the Congo basin. *Journal of African Earth Sciences* 43, 301-315.
- Govin, A., Holzwarth, U., Heslop, D., Ford Keeling, L., Zabel, M., Mulitza, S., Collins, J.A, Chiessi, C. M. (2012). Distribution of major elements in Atlantic surface sediments (36°N–49°S): Imprint of terrigenous input and continental weathering. *Geochemistry, Geophysics, Geosystems* 13, Q01013. doi:10.1029/2011GC003785
- Griffin, J.J., Windom, H., Goldberg, E.D. (1968). The distribution of clay minerals in the world ocean. In *Deep Sea Research and Oceanographic* 15, 433-459.
- Grimes, S.T., Collinson, M.E., Hooker, J.J., Matthey, D.P. (2008). Is small beautiful? A review of the advantages and limitations of using small mammal teeth and the

952 direct laser fluorination analysis technique in the isotope reconstruction of past
 953 continental climate change. *Palaeogeography, Palaeoclimatology, Palaeoecology*
 954 266, 39-50.
 955 Grossman, E.L. (2012). Applying oxygen isotope paleothermometry in deep time. *The*
 956 *Paleontological Society Papers* 18, 39-68.
 957 Grossman, E.L., Ku, T.L. (1986). Oxygen and carbon isotope fractionation in biogenic
 958 aragonite: temperature effects. *Chemical Geology: Isotope Geoscience Section*
 959 59, 59-74.
 960 Gu, X.X., Liu, J.M., Zheng, M. H., Tang, J. X., Qi, L. (2002). Provenance and tectonic setting
 961 of the Proterozoic turbidites in Hunan. South China: geochemical evidence.
 962 *Journal of Sedimentary Research* 72, 393-407.
 963 Guillocheau, F., Simon, B., Baby, G., Bessin, P., Robin, C., Dauteuil, O., (2018). Planation
 964 surfaces as a record of mantle dynamics: The case example of Africa. *Gondwana*
 965 *Research*, 53, 82-98.
 966 Guiraud, M., Buta-Neto, A., & Quesne, D. (2010). Segmentation and differential post-rift
 967 uplift at the Angola margin as recorded by the transform-rifted Benguela and
 968 oblique-to-orthogonal-rifted Kwanza basins. *Marine and Petroleum Geology* 27,
 969 1040-1068.
 970 Guo, Y., Yang, S., Su, N., Li, C., Yin, P., Wang, Z. (2018). Revisiting the effects of
 971 hydrodynamic sorting and sedimentary recycling on chemical weathering
 972 indices. *Geochimica et Cosmochimica Acta* 227, 48-63.

- 973 Haddon, I.G., McCarthy, T.S. (2005). The Mesozoic–Cenozoic interior sag basins of
974 Central Africa: The Late-Cretaceous–Cenozoic Kalahari and Okavango basins.
975 Journal of African Earth Sciences 43, 316-333.
- 976 Harnois, L. (1988). The CIW index: a new chemical index of weathering. Sedimentary
977 geology, 55 319-322.
- 978 Heilborn, M., Valeriano, C.M., Tassinari, C.C.G., Almeida, J., Tupinambá, M., Siga Jr, O.,
979 Trouw, R. (2008). Correlation of Neoproterozoic terranes between the Ribeira
980 Belt, SE Brazil and its African counterpart: comparative tectonic evolution and
981 open questions. In: Pankhurst, R. J., Trouw, R. A. J., Brito Neves, B.B., Wit, M.J.
982 (Eds.), West Gondwana: Pre-Cenozoic Correlations Across the South Atlantic
983 Region. Geological Society, London, Spec. Publ. 294, pp. 211–237.
- 984 Hessler, A.M., Zhang, J., Covault, J., Ambrose, W. (2017). Continental weathering
985 coupled to Paleogene climate changes in North America. Geology 45, 911-914.
- 986 Hodell, D.A., Brenner, M., Kanfoush, S.L., Curtis, J.H., Stoner, J.S., Xueliang, S., ... ,
987 Whitmore, T. J. (1999). Paleoclimate of southwestern China for the past 50,000
988 yr inferred from lake sediment records. Quaternary Research 52, 369-380.
- 989 Hong, H., Li, Z., Xue, H., Zhu, Y., Zhang, K., Xiang, S. (2007). Oligocene clay mineralogy of
990 the Linxia Basin: evidence of paleoclimatic evolution subsequent to the initial-
991 stage uplift of the Tibetan Plateau. Clays and Clay Minerals 55, 491-503.
- 992 Hundert, T., Piper, D.J.W., Pe-Piper, G. 2006. Genetic model and exploration guidelines
993 for kaolin beneath unconformities in the Lower Cretaceous fluvial Chaswood
994 Formation, Nova Scotia. Exploration and Mining Geology 15, 9-26.

- 2597
2598
2599 995 Jackson, M.P.A, Hudec, M.R., Hegarty, K.A. (2005). The great West African Tertiary
2600
2601 996 coastal uplift: fact or fiction? A perspective from the Angolan divergent margin.
2602
2603 Tectonics, 24, TC6014, doi:10.1029/2005TC001836.
2604 997
2605
2606 998 Jaffrés, J.B., Shields, G.A., Wallmann, K. (2007). The oxygen isotope evolution of
2607
2608 999 seawater: A critical review of a long-standing controversy and an improved
2609
2610 geological water cycle model for the past 3.4 billion years. Earth-Science Reviews
2611 1000
2612 83, 83-122.
2613 1001
2614
2615 1002 Jansen, N., Hartmann, J., Lauerwald, R., Dürr, H.H., Kempe, S., Loos, S., Middelkoop, H.
2616
2617 (2010). Dissolved silica mobilization in the conterminous USA. Chemical Geology
2618 1003
2619 270, 90-109.
2620 1004
2621
2622 1005 Johnsson, M.J. and Meade, R.H. (1990). Chemical weathering of fluvial sediments during
2623
2624 alluvial storage: The Macuapanim Island point bar, Solimões River, Brazil. Journal
2625 1006
2626 of Sedimentary Petrology, 60, 827-842.
2627 1007
2628
2629 1008 Kadima, E., Delvaux, D., Sebagenzi, S. N., Tack, L., Kabeya, S. M. (2011). Structure and
2630
2631 geological history of the Congo Basin: an integrated interpretation of gravity,
2632 1009
2633 magnetic and reflection seismic data. Basin Research 23, 499-527.
2634 1010
2635
2636 1011 Kahle, M., Kleber, M., Jahn, R. (2002). Review of XRD-based quantitative analyses of clay
2637
2638 minerals in soils: the suitability of mineral intensity factors. Geoderma 109, 191-
2639 1012
2640 205.
2641 1013
2642
2643 1014 Kalm, V.E., Rutter, N.W., Rokosh, C.D. (1996). Clay minerals and their
2644
2645 paleoenvironmental interpretation in the Baoji loess section, Southern Loess
2646 1015
2647 Plateau, China. Catena 27, 49-61.
2648 1016
2649
2650
2651
2652
2653
2654
2655

- 1017 Klingebiel, A. (1963). Observations sur la sédimentation argileuse du début des temps
1018 tertiaires en Aquitaine. Bulletin de la Société Géologique de France 7, 303-306.
- 1019 Kobashi, T., Grossman, E.L., Yancey, T. E., Dockery III, D.T. (2001). Reevaluation of
1020 conflicting Eocene tropical temperature estimates: Molluscan oxygen isotope
1021 evidence for warm low latitudes. Geology 29, 983-986.
- 1022 Köhn, M. (1928). Bemerkungen zur mechanischen Bodenanalyse. III. Ein neuer
1023 Pipettapparat. Zeitschrift für Pflanzenernährung, Düngung, Bodenkunde 11, 50-
1024 54.
- 1025 Kump, L.R., Brantley, S.L., Arthur, M.A. (2000). Chemical weathering, atmospheric CO₂,
1026 and climate. Annual Review of Earth and Planetary Sciences 28, 611-667.
- 1027 Leng, M.J., Marshall, J.D. (2004). Palaeoclimate interpretation of stable isotope data
1028 from lake sediment archives. Quaternary Science Reviews 23, 811-831.
- 1029 Liu, J., Chen, J., Selvaraj, K., Xu, Q., Wang, Z., Chen, F. (2014). Chemical weathering over
1030 the last 1200 years recorded in the sediments of Gonghai Lake, Lvliang
1031 Mountains, North China: a high-resolution proxy of past climate. Boreas 43, 914-
1032 923.
- 1033 Louvat, P., Gislason, S.R., Allègre, C.J., 2008. Chemical and mechanical erosion rates in
1034 Iceland as deduced from river dissolved and solid material. American Journal of
1035 Science 308, 679-726.
- 1036 Marzoli, A., Melluso, L., Morra, V., Renne, P.R., Sgroso, I., D'Antonio, M., Duarte, L.,
1037 Morais, E.A.A., Ricci, G. (1999). Geochronology and petrology of Cretaceous
1038 basaltic magmatism in the Kwanza basin (western Angola), and relationship with

- 1039 the Paraná-Etendeka continental flood basalt province. *Journal of Geodynamics*
- 1040 28, 341-356.
- 1041 Mayer, A., Hofmann, A.W., Sinigoi, S., Morais, E. (2004). Mesoproterozoic Sm-Nd and
- 1042 U-Pb ages for the Kunene anorthosite complex of SW Angola. *Precambrian*
- 1043 *Research* 133, 187-206.
- 1044 Maynard, J.B. (1992). Chemistry of modern soils as a guide to interpreting Precambrian
- 1045 paleosols. *The Journal of Geology* 100, 279-289.
- 1046 Minasny, B., Finke, P., Stockmann, U., Vanwalleghem, T., McBratney, A.B. (2015).
- 1047 Resolving the integral connection between pedogenesis and landscape
- 1048 evolution. *Earth-Science Reviews* 150, 102-120.
- 1049 McDermott, F. (2004). Palaeo-climate reconstruction from stable isotope variations in
- 1050 speleothems: a review. *Quaternary Science Reviews* 23, 901-918.
- 1051 Meunier, A., Caner, L., Hubert, F., El Albani, A. and Prêt, D., 2013. The weathering
- 1052 intensity scale (WIS): an alternative approach of the chemical index of alteration
- 1053 (CIA). *American journal of science*, 313(2), pp.113-143.
- 1054 Meybeck, M. (1987). Global chemical weathering of surficial rocks estimated from river
- 1055 dissolved loads. *American journal of science* 287, 401-428.
- 1056 Moore, D., Reynolds, R. (1997). X-Ray-Diffraction and the identification and analysis of
- 1057 clay minerals. Oxford University Press, New York.
- 1058 Moquet, J.S., Crave, A., Viers, J., Seyler, P., Armijos, E., Bourrel, L., Chavarri, E., Lagane,
- 1059 C., Laraque, A., Casimiro, W.S.L, Pombosa, R., Noriega, L, Vera, A., Guyot, J.-L.

2774
2775
2776 1060 (2011). Chemical weathering and atmospheric/soil CO₂ uptake in the Andean
2777
2778 and Foreland Amazon basins. Chemical Geology 287, 1-26.
2779 1061
2780
2781 1062 Moulin, M., Aslanian, D., Unternehr, P. (2010). A new starting point for the South and
2782
2783 Equatorial Atlantic Ocean. Earth-Science Reviews 98, 1-37.
2784 1063
2785
2786 1064 Nesbitt, H.W., Young, G.M. (1982). Early Proterozoic climates and plate motions inferred
2787
2788 from major element chemistry of lutites. Nature 299, 715-717.
2789 1065
2790
2791 1066 Noller, J.S., Sowers, J.M., & Lettis, W.R. (Eds.). (2000). Quaternary geochronology:
2792
2793 methods and applications (Vol. 4). American Geophysical Union.
2794 1067
2795
2796 1068 Parker, A. (1970). An index of weathering for silicate rocks. Geological Magazine, 107,
2797
2798 501-504.
2799 1069
2800
2801 1070 Peel, M.C., Finlayson, B.L., McMahon, T.A. (2007). Updated world map of the Koppen-
2802
2803 Geiger climate classification. Hydrology and Earth System Sciences 11, 1633-
2804 1071
2805 1644.
2806 1072
2807
2808 1073 Petschick, R., Kuhn, G., Gingele, F. (1996). Clay mineral distribution in surface sediments
2809
2810 of the South Atlantic: sources, transport, and relation to oceanography. Marine
2811 1074
2812 Geology 130, 203-229.
2813 1075
2814
2815 1076 Power, P.E. (1969). Clay mineralogy and paleoclimatic significance of some red regoliths
2816
2817 and associated rocks in western Colorado. Journal of Sedimentary Research 39,
2818 1077
2819 876-890
2820 1078
2821
2822 1079 Riebe, C.S., Kirchner, J.W., Finkel, R.C. (2004). Erosional and climatic effects on long-term
2823
2824 chemical weathering rates in granitic landscapes spanning diverse climate
2825 1080
2826 regimes. Earth and Planetary Science Letters 224, 547-562.
2827 1081
2828
2829
2830
2831
2832

- 1082 Rieu, R., Allen, P. A., Plotze, M., & Pettke, T. (2007). Compositional and mineralogical
1083 variations in a Neoproterozoic glacially influenced succession, Mirbat area, south
1084 Oman: Implications for paleoweathering conditions. *Precambrian Research* 154,
1085 248-265.
- 1086 Rouse, H., 1937. Modern conceptions of the mechanics of fluid turbulence. *Transactions*
1087 *of the American Society of Civil Engineers* 102, 463-543.
- 1088 Roy, P.D., Caballero, M., Lozano, R., Smykatz-Kloss, W (2008). Geochemistry of late
1089 Quaternary sediments from Tecocomulco lake, central Mexico: Implication to
1090 chemical weathering and provenance. *Chem. Erde Geochem.* 68, 383-393.
- 1091 Royer, A., Lécuyer, C., Montuire, S., Amiot, R., Legendre, S., Cuenca-Bescós, G., ...,
1092 Martineau, F. (2013). What does the oxygen isotope composition of rodent teeth
1093 record? *Earth and Planetary Science Letters* 361, 258-271.
- 1094 Rufyikiri, G., Nootens, D., Dufey, J.E., Delvaux, B. (2004). Mobilization of aluminium and
1095 magnesium by roots of banana (*Musa spp.*) from kaolinite and smectite clay
1096 minerals. *Applied Geochemistry* 19, 633-643.
- 1097 Sardans, J., Penuelas, J., Ogaya, R. (2008). Drought's impact on Ca, Fe, Mg, Mo and S
1098 concentration and accumulation patterns in the plants and soil of a
1099 Mediterranean evergreen *Quercus ilex* forest. *Biogeochemistry* 87, 49-69.
- 1100 Schmitz, B., Andreasson, F.P. (2001). Air humidity and lake $\delta^{18}\text{O}$ during the latest
1101 Paleocene-earliest Eocene in France from recent and fossil fresh-water and
1102 marine gastropod $\delta^{18}\text{O}$, $\delta^{13}\text{C}$, and $87\text{Sr}/86\text{Sr}$. *Geological Society of America*
1103 *Bulletin* 113, 774-789.

- 1104 Schulz H., cruise participants, 1992. Bericht und erste Ergebnisse über die METEOR Fahrt
- 1105 M 20-1, Abidjan – Dakar, 131 pp., Berichte, Fachbereich Geowissenschaften,
- 1106 Universität Bremen, No. 25,173.
- 1107 Séranne, M., Anka, Z. (2005). South Atlantic continental margins of Africa: a comparison
- 1108 of the tectonic vs climate interplay on the evolution of equatorial west Africa and
- 1109 SW Africa margins. *Journal of African Earth Sciences* 43, 283-300.
- 1110 Sheldon, N.D., Tabor, N.J. (2009). Quantitative paleoenvironmental and paleoclimatic
- 1111 reconstruction using paleosols. *Earth-science Reviews* 95, 1-52.
- 1112 Šimkevičius, P., Ahlberg, A., Grigelis, A. (2003). Jurassic smectite and kaolinite trends of
- 1113 the East European Platform: implications for palaeobathymetry and
- 1114 palaeoclimate. *Terra Nova* 15, 225-229.
- 1115 Sittler, C., Millot, G. (1964). Les climats du Paléogène français reconstitués par les argiles
- 1116 néoformées et les microflores. *Geologische Rundschau* 54, 333-343.
- 1117 Tack, L., Wingate, M.T.D., Liégeois, J.P., Fernandez-Alonso, M., Deblond, A. (2001). Early
- 1118 Neoproterozoic magmatism (1000–910 Ma) of the Zadinian and Mayumbian
- 1119 Groups (Bas-Congo): onset of Rodinia rifting at the western edge of the Congo
- 1120 craton. *Precambrian Research* 110, 277-306.
- 1121 Vanoni, V.A., 2006. Sedimentation engineering. Am. Soc. Civ. Eng., Reston: ASCE
- 1122 Manuals and Reports in Engineering Practice, 54. 418 p.
- 1123 Vaughan, A.P., Pankhurst, R.J. (2008). Tectonic overview of the West Gondwana margin.
- 1124 Gondwana Research 13, 150-162.

2951
2952
2953
2954
2955
2956
2957
2958
2959
2960
2961
2962
2963
2964
2965
2966
2967
2968
2969
2970
2971
2972
2973
2974
2975
2976
2977
2978
2979
2980
2981
2982
2983
2984
2985
2986
2987
2988
2989
2990
2991
2992
2993
2994
2995
2996
2997
2998
2999
3000
3001
3002
3003
3004
3005
3006
3007
3008
3009

1125 Vermeesch, P., Resentini, A. and Garzanti, E., 2016. An R package for statistical
1126 provenance analysis. *Sedimentary Geology*, doi:10.1016/j.sedgeo.2016.01.009.

1127 Viers, J., Dupré, B., & Gaillardet, J. (2009). Chemical composition of suspended
1128 sediments in World Rivers: New insights from a new database. *Science of the*
1129 *total Environment* 407, 853-868.

1130 von Eynatten, H., Tolosana-Delgado, R., & Karius, V. (2012). Sediment generation in
1131 modern glacial settings: grain-size and source-rock control on sediment
1132 composition. *Sedimentary Geology* 280, 80-92.

1133 von Eynatten, H., Tolosana-Delgado, R., Karius, V., Bachmann, K., Caracciolo, L. (2016).
1134 Sediment generation in humid Mediterranean setting: Grain-size and source-
1135 rock control on sediment geochemistry and mineralogy (Sila Massif, Calabria).
1136 *Sedimentary Geology* 336, 68-80.

1137 Walker, J.C., Hays, P.B., Kasting, J.F. (1981). A negative feedback mechanism for the
1138 long-term stabilization of Earth's surface temperature. *Journal of Geophysical*
1139 *Research: Oceans* 86(C10), 9776-9782.

1140 Weaver, C. E. (1989). Clays, muds, and shales. *Developments in Sedimentology* 44.
1141 Elsevier.

1142 Wefer, G., cruise participants, 1988. Bericht über METEOR Fahrt M 6-6, Libre Ville – Las
1143 Palmas, 97 pp., Berichte, Fachbereich Geowissenschaften, Universität Bremen,
1144 No. 3.

1145 West, A. J., Galy, A., Bickle, M. (2005). Tectonic and climatic controls on silicate
1146 weathering. *Earth and Planetary Science Letters* 235, 211-228.

- 1147 West. A.J., Bickle, M.J., Collins, R., Brasington, J. (2002) Small-catchment perspective on
1148 Hymalayan eathering fluxes. *Geology* 30, 355-358.
- 1149 White, A.F. and Blum, A.E. (1995). Effects of climate on chemical weathering in
1150 watersheds. *Geochimica and Cosmochimica Acta* 59, 1729-1747.
- 1151 Wierzbowski, H., Rogov, M.A., Matyja, B.A., Kiselev, D., Ippolitov, A. (2013). Middle-
1152 Upper Jurassic (Upper Callovian–Lower Kimmeridgian) stable isotope and
1153 elemental records of the Russian Platform: indices of oceanographic and climatic
1154 changes. *Global and Planetary Change* 107, 196-212.
- 1155 Wiggs, G.F., Thomas, D. S., Bullard, J.E., Livingstone, I. (1995). Dune mobility and
1156 vegetation cover in the southwest Kalahari Desert. *Earth Surface Processes and*
1157 *Landforms* 20, 515-529.
- 1158 Yan, Y, Xia, B, Lin, G, Cui, X, Hu X, Yan, P., Zhang, F. (2007). Geochemistry of the
1159 sedimentary rocks from the Nanxiong Basin, South China and implications for
1160 provenance, paleoenvironment and paleoclimate at the K/T boundary.
1161 *Sedimentary Geology* 197, 127–140.
- 1162 Yang, S., Jung, H. S., Li, C. (2004). Two unique weathering regimes in the Changjiang and
1163 Huanghe drainage basins: geochemical evidence from river sediments.
1164 *Sedimentary Geology* 164, 19-34.
- 1165 Zachos, J., Pagani, M., Sloan, L., Thomas, E., Billups, K. (2001). Trends, rhythms, and
1166 aberrations in global climate 65 Ma to present. *Science* 292, 686-693.
- 1167
- 1168

Figure captions

Fig. 1: General features of the study area. (A) Location in Southern Africa; the dotted line indicates the areas studied in Petschick et al. (1996) and Garzanti et al. (2013, 2014), whose data are used in the present research. (B) Topography, and location of fluvial and offshore samples in which the geochemistry of two size fractions and clay mineralogy were determined. Numbers for marine samples refer to the GeoB cores. (C) Rainfall (mm) and (D) temperature (°C) in the Congo River basin and along the SW African Atlantic margin (from Fick and Hijmans, 2017).

Fig. 2: Schematic geological map of the SW Africa Atlantic Margin and Congo River basin. Based on CGMW-BRGM (2016). LCB: Lower Congo Basin; KB: Kwanza Basin; NB: Namibe Basin. Drainage basins investigated in this study are outlined.

Fig. 3: Chemical composition of river muds. (A) Ratio between element concentrations in the < 2 µm and < 32 µm fractions, (B) Range of values for the two mud fractions in the lower Congo and SW Atlantic margin, (C) Range of values for upper Congo (<63 µm fraction) and Namibia (<32 µm fraction). Element concentrations are normalized to the

UCC and the chemical elements are ranked on the X-axis according to their increasing enrichment relative to the UCC (Rudnick and Gao, 2003; Hu and Gao 2008).

Fig. 4: Map of the principal components for a selection of chemical elements of the <32 μm (A) and <2 μm (B) fractions. PCA performed with the provenance R-package (Vermeesch et al., 2016). Geochemical data were subjected to a centred log-ratio transformation in order to remove the unit-sum constraint (Aitchison, 1986). The vector loadings of the PCA for the <32 μm fraction define two perpendicular links, indicating two independent controls on the data (Aitchison and Greenacre, 2002). The first link connects the mobile elements (Ca, Na, Al and Ti) and is attributed to weathering (blue). The second link connects elements (Mg, Mn, Co, Th, U, W, LREE) that are linked to source rock geology (brown). These two components are less visible in the fine fraction (<2 μm).

Fig. 5: Comparison of the levels of depletion/enrichment in different elements relative to the UCC ($\alpha_{\text{E}}^{\text{Al}}$) in the <2 μm and <32 μm fractions of river muds. (A and B) Average values of $\alpha_{\text{E}}^{\text{Al}}$ in the <2 μm and <32 μm fractions. Na, followed distantly by Ca and Sr, is the most depleted element. Non-mobile elements may show values higher than 1 where Al concentration is even higher. The size of the circle diameter is proportional to the observed correlation between the <2 μm and <32 μm fractions. The lack of correlation for CaO is strongly conditioned by the anomalous low Ca content in the

1213 Congo Estuary ($r=0.92$ if this sample is excluded). (C) Coefficient of variation (CV =
 1214 standard deviation divided by the mean) of α_E^{Al} indices for different elements in the <2
 1215 μm and $<32 \mu m$ fractions. Higher variability in the $<32 \mu m$ fraction may be caused by
 1216 hydraulic-sorting processes responsible for variable concentration of heavy minerals; P
 1217 concentration in the finer fraction may reveal uptake by plants. (D) Levels of depletion
 1218 in Zr (α_{Zr}^{Al}) in muds from different regions. Far better correlations occur if muds
 1219 collected at different latitudes are isolated.

1222 Fig. 6: Variation with water depth of different compositional features of offshore
 1223 marine muds. (A) Si/Al and concentration of TiO_2 and Zr in the $<5 \mu m$ fraction. (B)
 1224 Levels of depletion in Mg (α_{Mg}^{Al}) and K (α_K^{Al}) and CIA in the $<5 \mu m$ fraction. Levels of
 1225 depletion in Mg and K and CIA in the $<63 \mu m$ fraction.

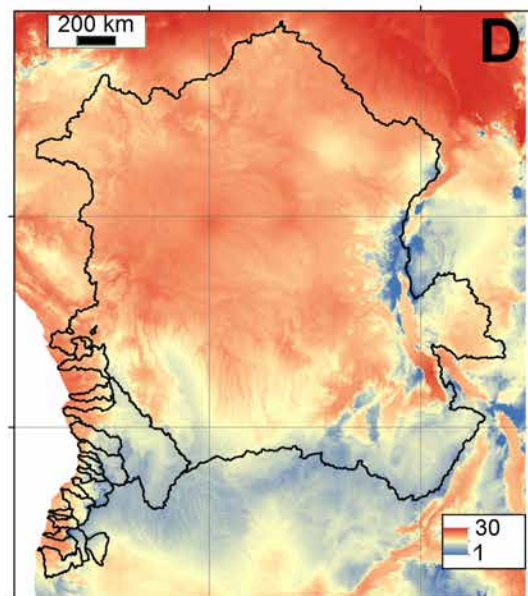
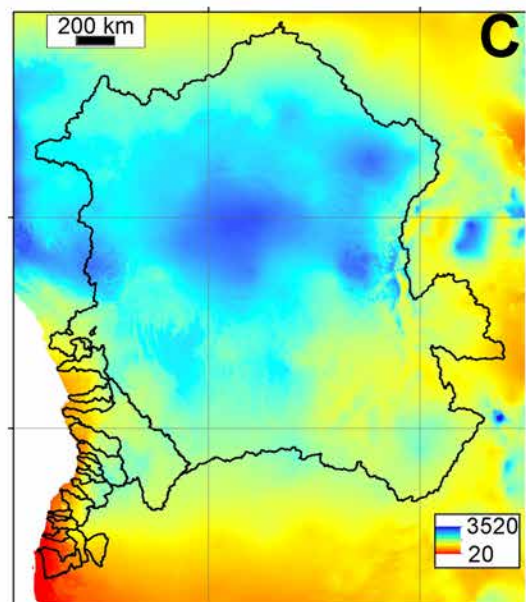
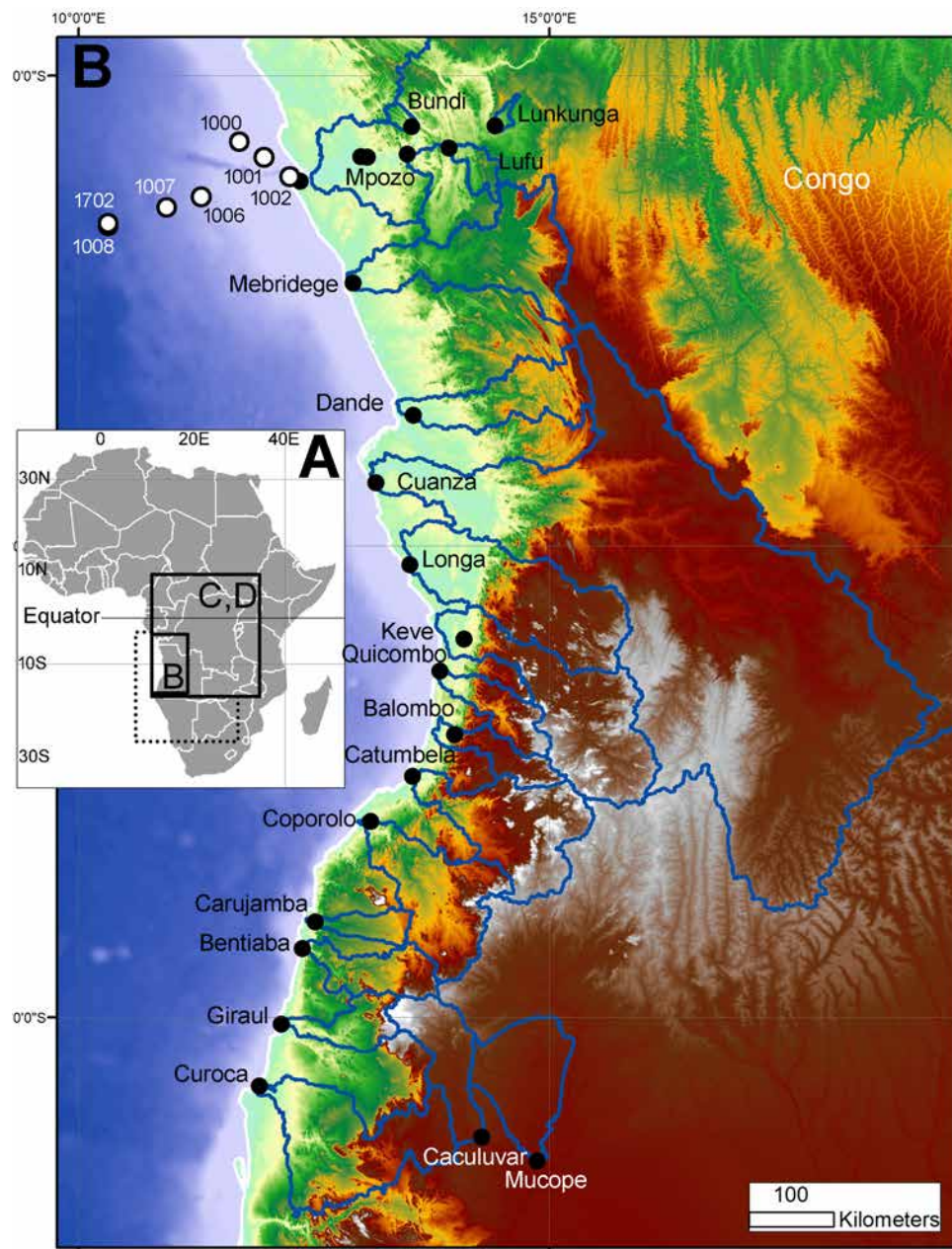
1228 Fig. 7: Clay mineral assemblages in river muds and marine deposits from Southern
 1229 Africa (A). Temperate/arid steppe and arid Namibia samples from Garzanti et al.
 1230 (2014); equatorial upper Congo samples from Garzanti et al. (2013); offshore samples
 1231 from Petschick et al. (1996). Variation in smectite content in offshore samples with
 1232 water depth in equatorial ($<12.5^\circ$ latitude; B) and sub-tropical ($>12.5^\circ$ latitude; C)

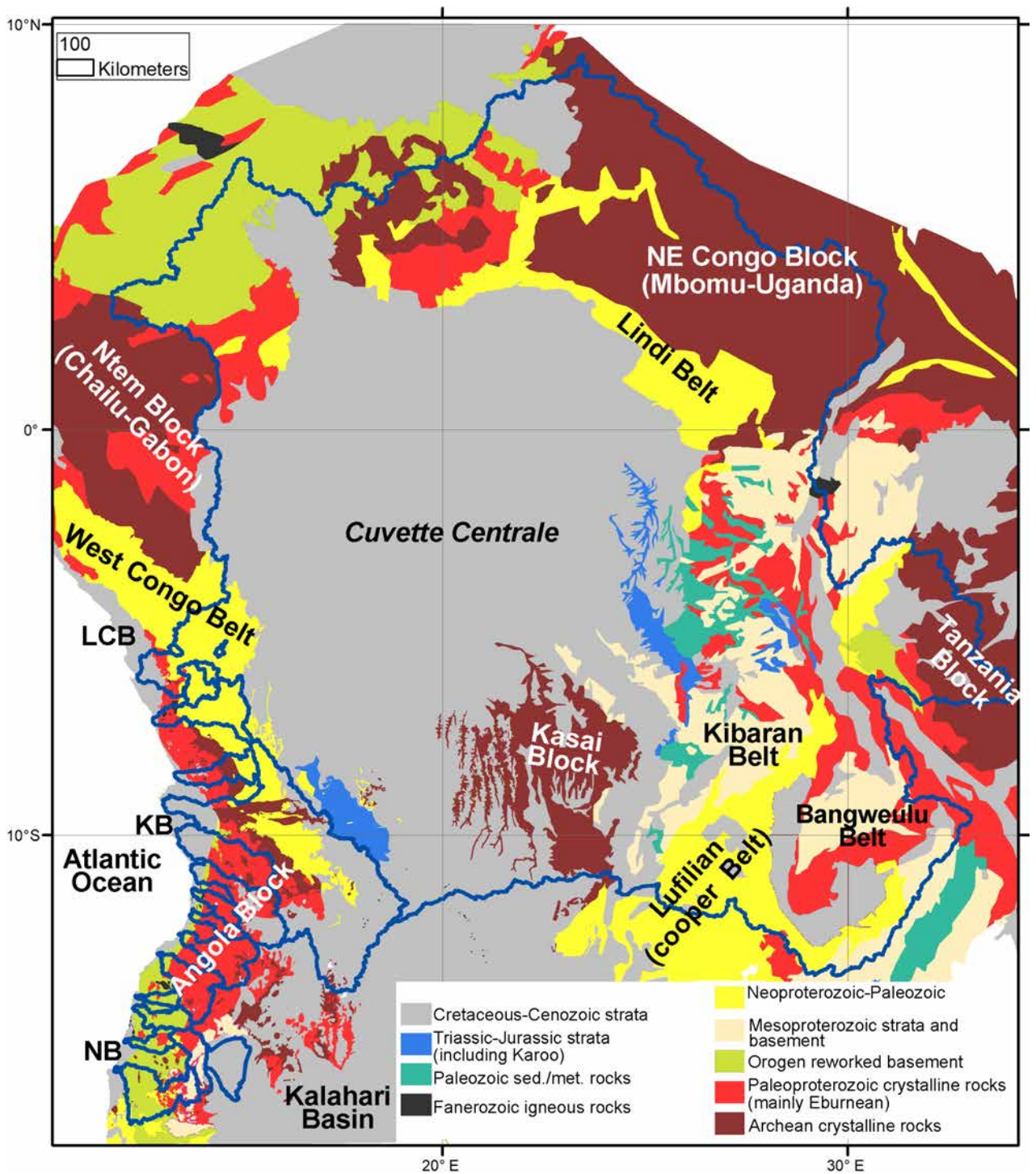
Fig. 8: Relations between average annual rainfall in the catchment and diverse compositional parameters of river muds from Southern Africa (0-30° latitude). CIA (A), WIP (B) and the level of depletion in Mg ($\alpha_{\text{Mg}}^{\text{Al}}$) (C) were obtained for the <32 μm fraction, with the exception of samples from equatorial upper Congo (<63 μm). Kaolinite proportion in the clay assemblage (D) was determined in the <2 μm fraction for all samples. Equatorial upper Congo and temperate/arid steppe and arid Namibia samples from Garzanti et al. (2013, 2014). Samples from upper Congo are neglected in the calculation of regression lines for geochemical data (CIA, WIP and $\alpha_{\text{Mg}}^{\text{Al}}$).

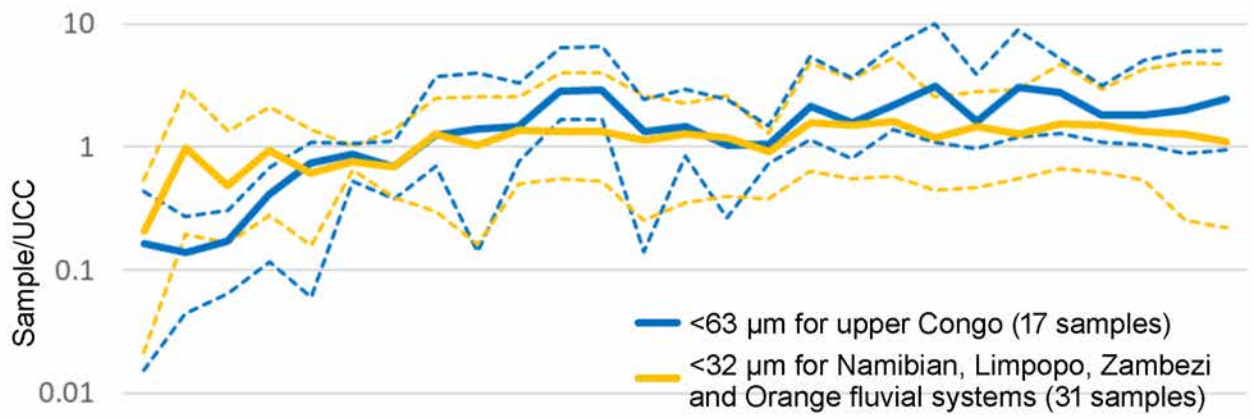
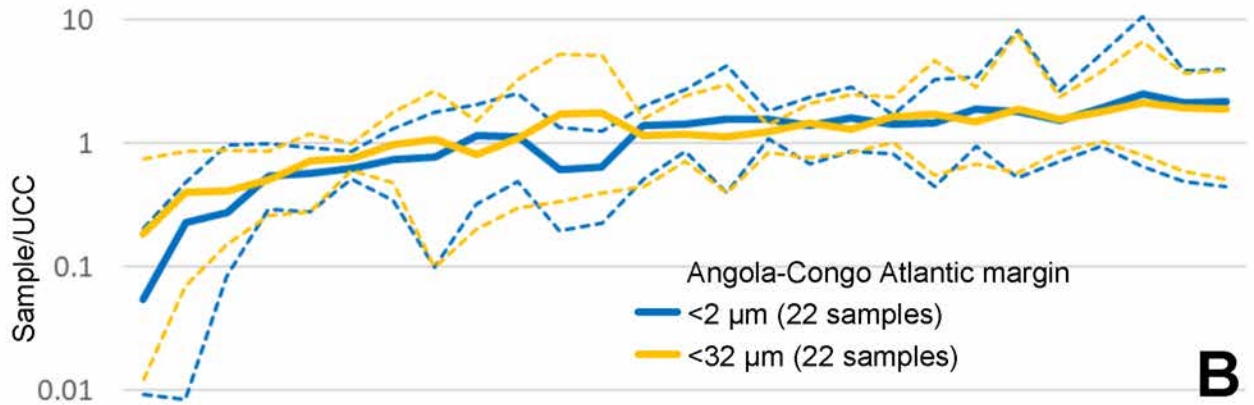
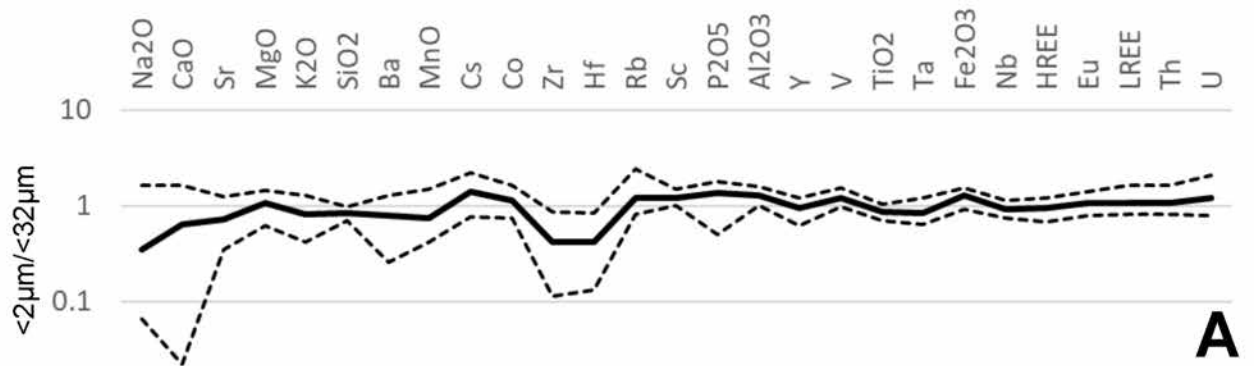
Fig. 9: Relations between average annual rainfall in the catchment and weathering indices determined from the <2 μm fraction. For geochemical data the dispersion can be reduced if both smaller rivers (drainage area < 2000 km^2) and the huge Congo basin are neglected.

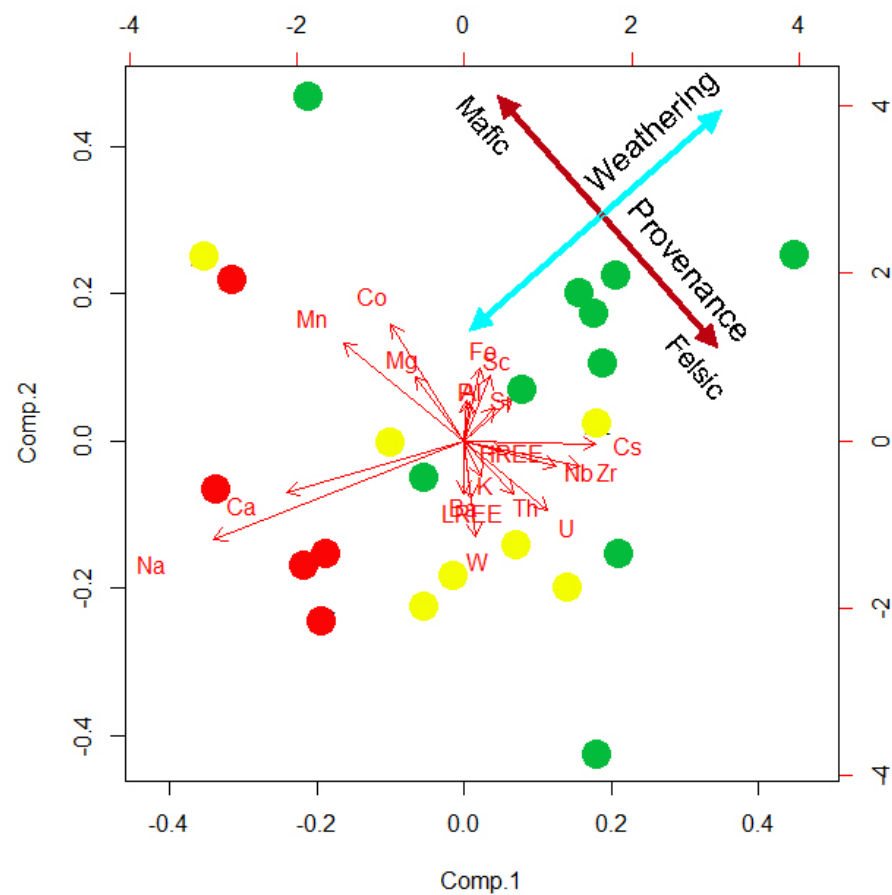
Fig. 10: Link between the ratio of Na-depletion in the <2 μm and <32 μm fractions ($(\alpha_{\text{Na}}^{\text{Al}})_2 / (\alpha_{\text{Na}}^{\text{Al}})_{32}$) and the areal proportion of Meso-Cenozoic sedimentary units in the respective catchments (A). Mucope sand is entirely derived from recycled Kalahari sand. Recycled detritus chiefly consisting of quartz is also overwhelming in Congo and Congo estuary sand and Caculuar River (Garzanti et al., 2018b and This Volume). The large majority of river muds in inset (B) are either from arid to semi-arid settings in

3305		
3306		
3307	1257	coastal southwestern Angola (Curoca, Giraul, Bentiaba, and Carujamba) or from humid
3308		
3309	1258	settings in northwestern Angola and Bas-Congo draining the West Congo Belt
3310		
3311		
3312	1259	(Mebridege, Lufu, Lunkunga, Mpozo and Bundi); other sources of recycled material
3313		
3314	1260	besides Meso-Cenozoic sedimentary units can be considered for these rivers.
3315		
3316		
3317	1261	
3318		
3319		
3320	1262	Table captions
3321		
3322		
3323	1263	Table 1. A selection of compositional parameters that may reflect weathering intensity.
3324		
3325	1264	(1) Use molar proportions; (2) Uses monocationic millimoles.
3326		
3327		
3328		
3329		
3330		
3331		
3332		
3333		
3334		
3335		
3336		
3337		
3338		
3339		
3340		
3341		
3342		
3343		
3344		
3345		
3346		
3347		
3348		
3349		
3350		
3351		
3352		
3353		
3354		
3355		
3356		
3357		
3358		
3359		
3360		
3361		
3362		
3363		

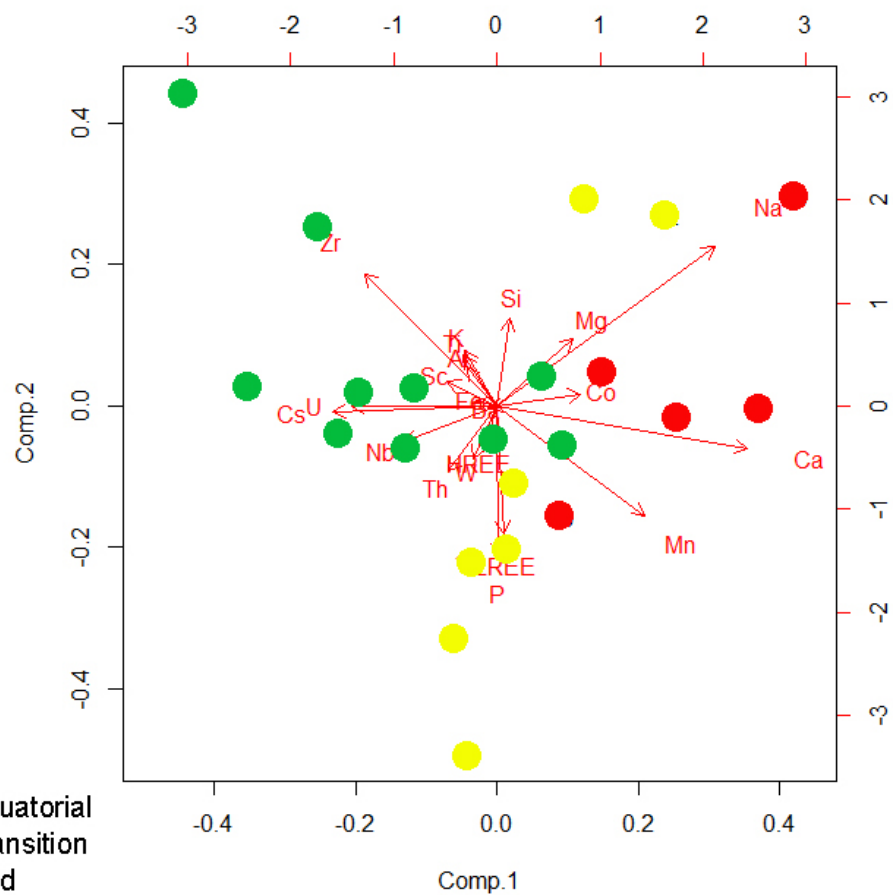


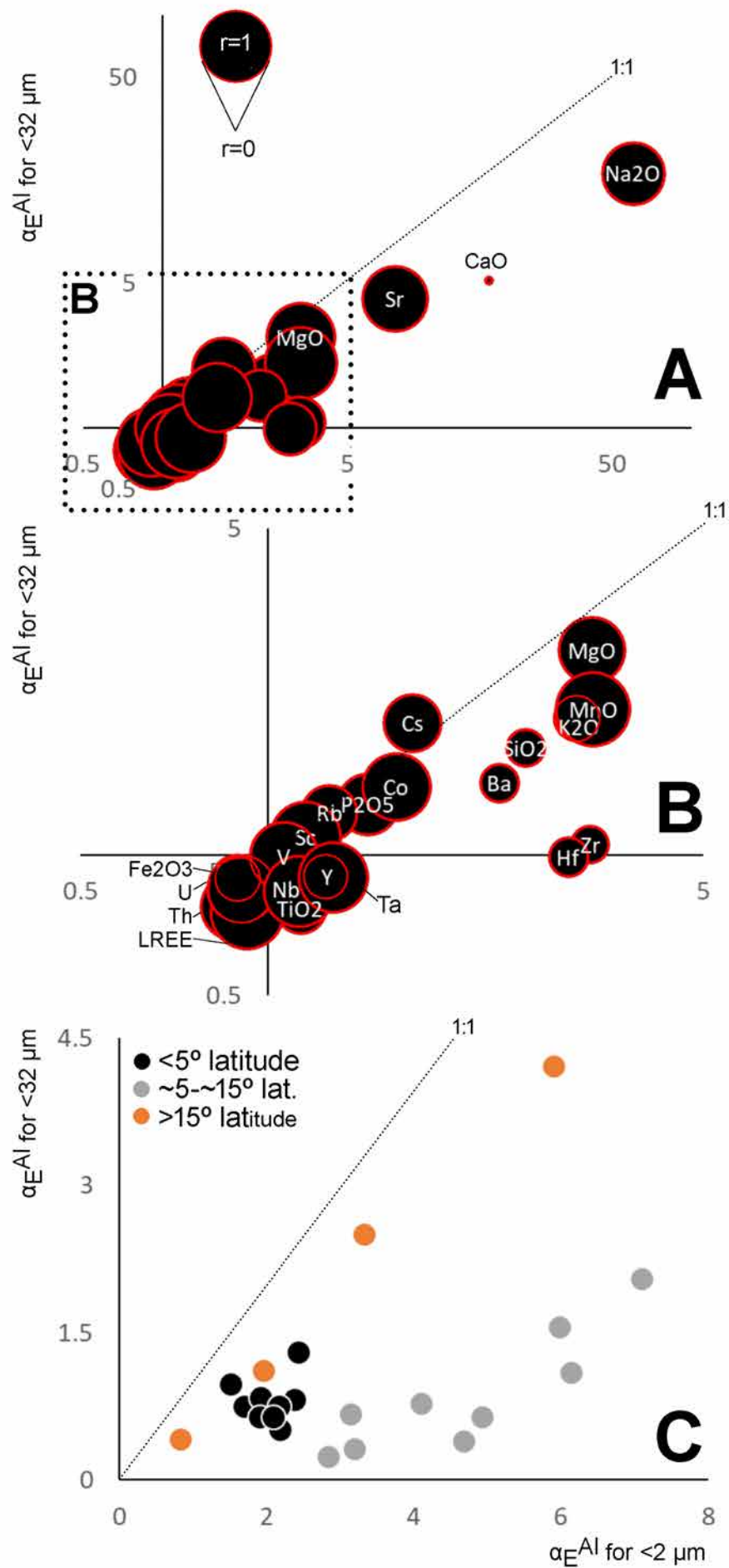


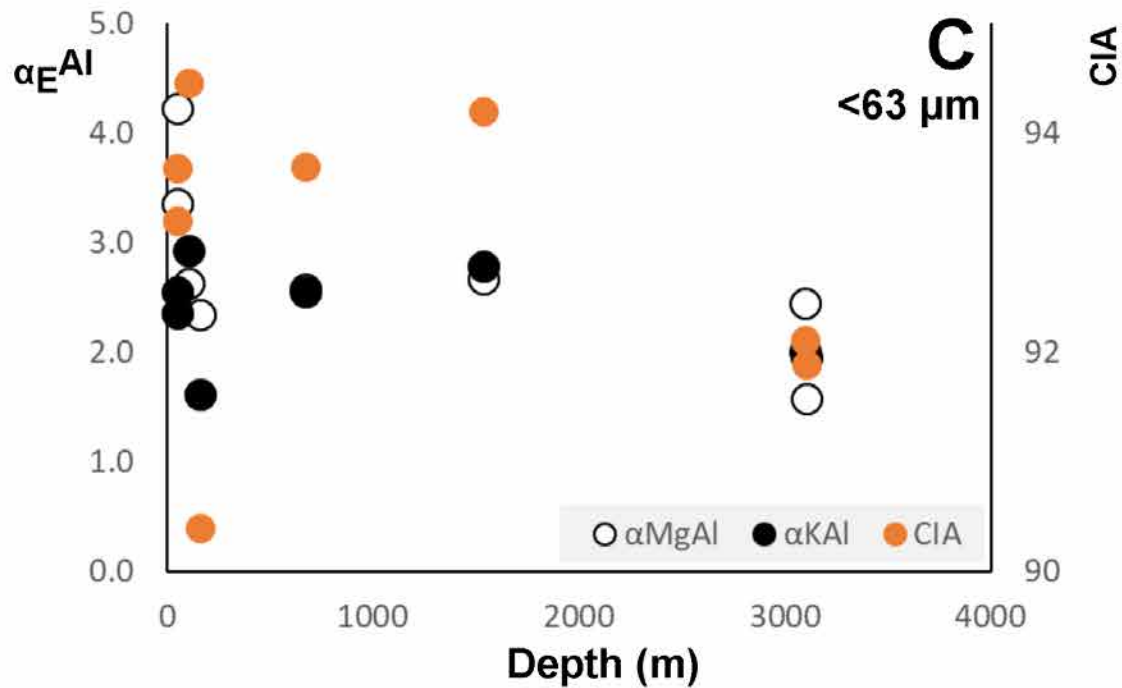
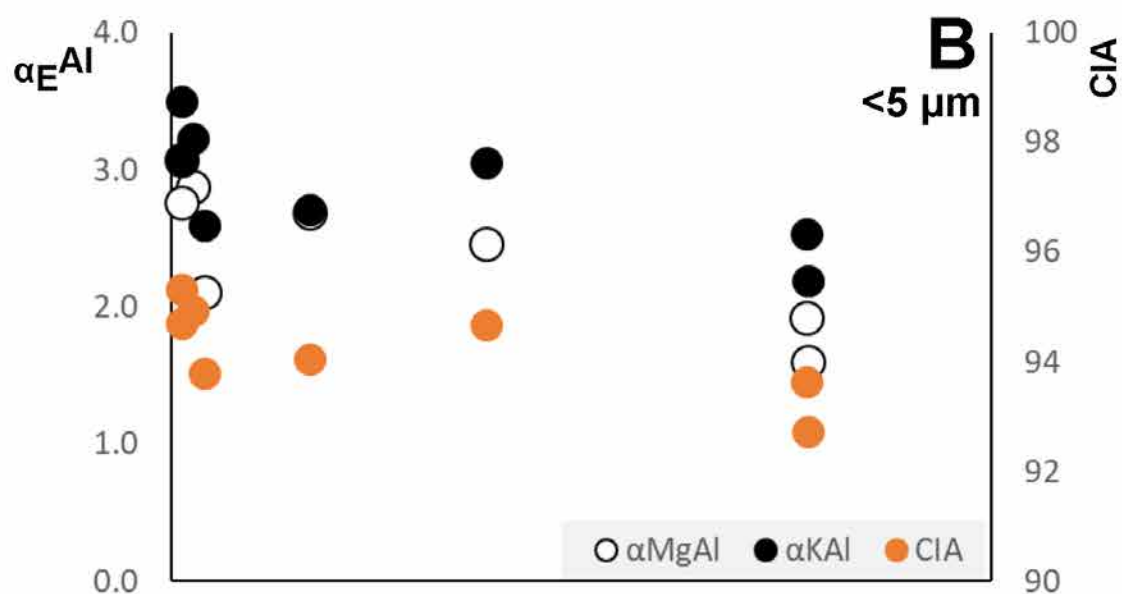
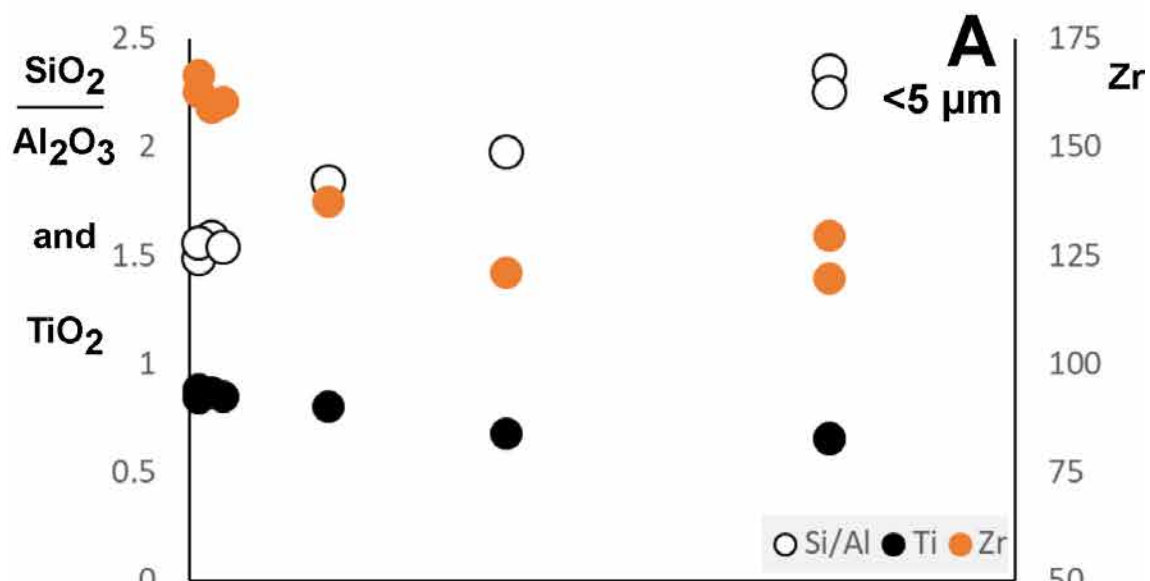


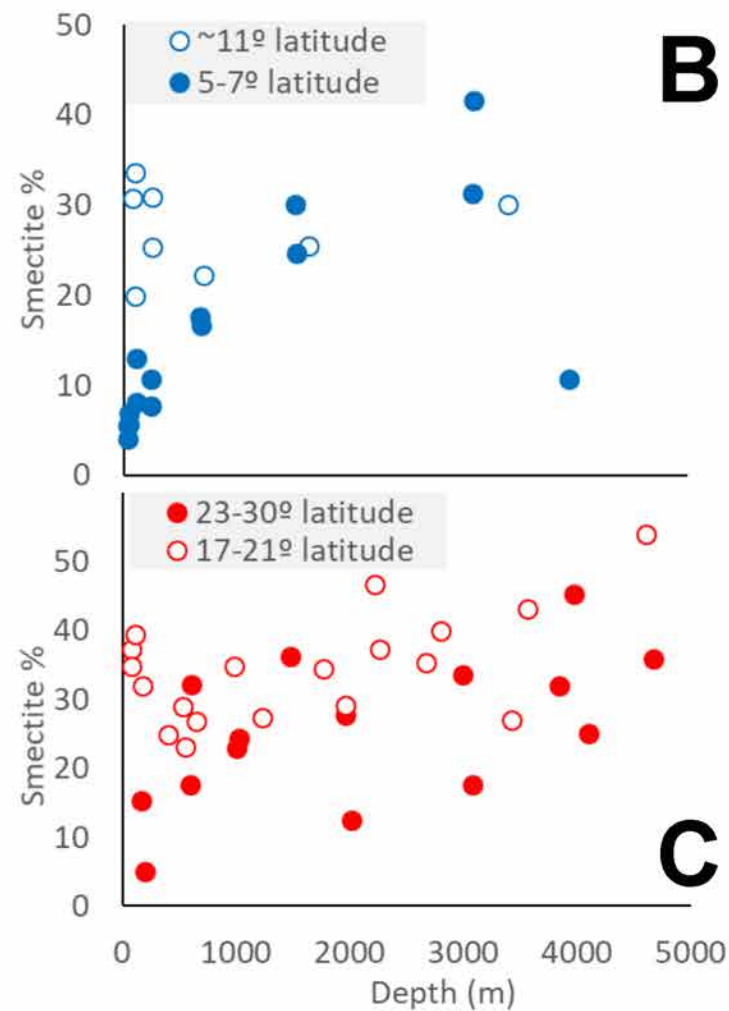
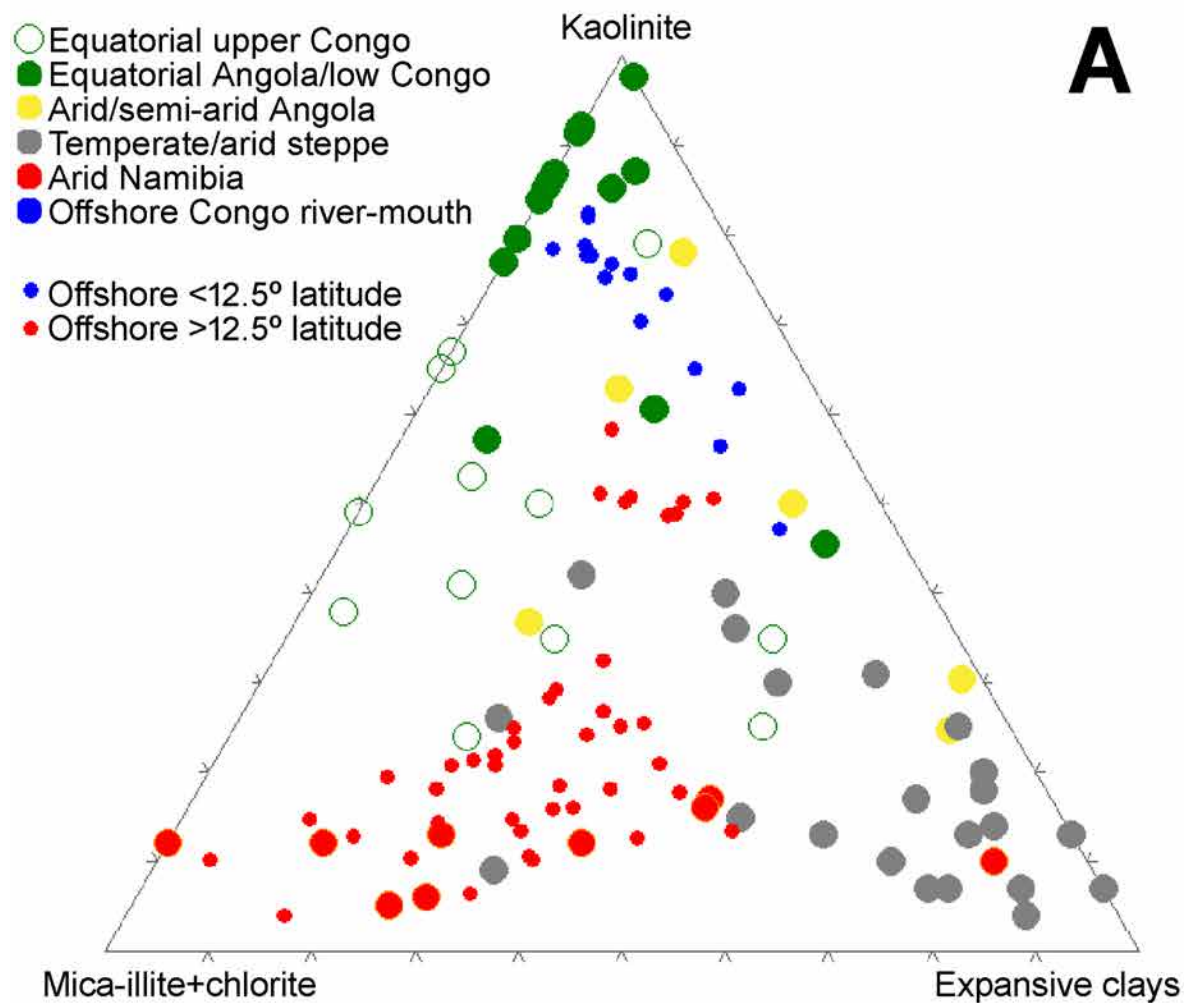


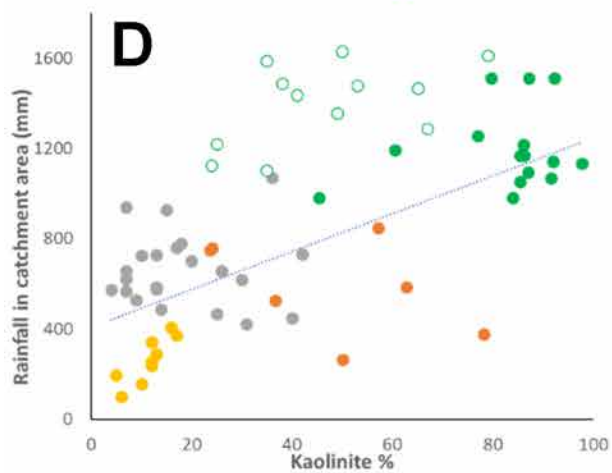
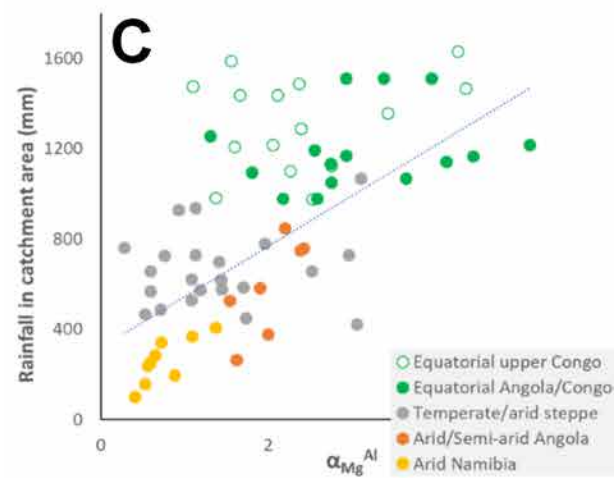
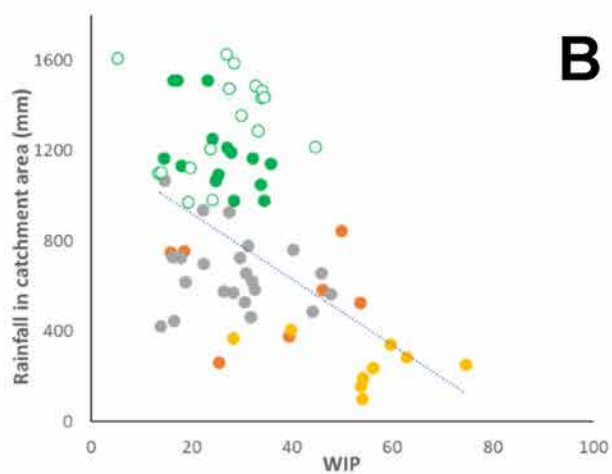
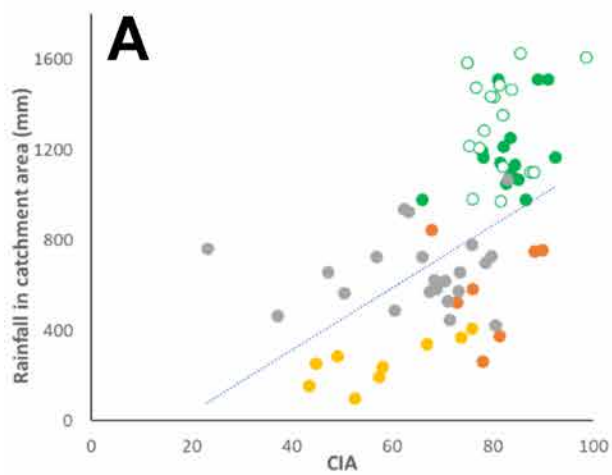
● Equatorial
● Transition
● Arid

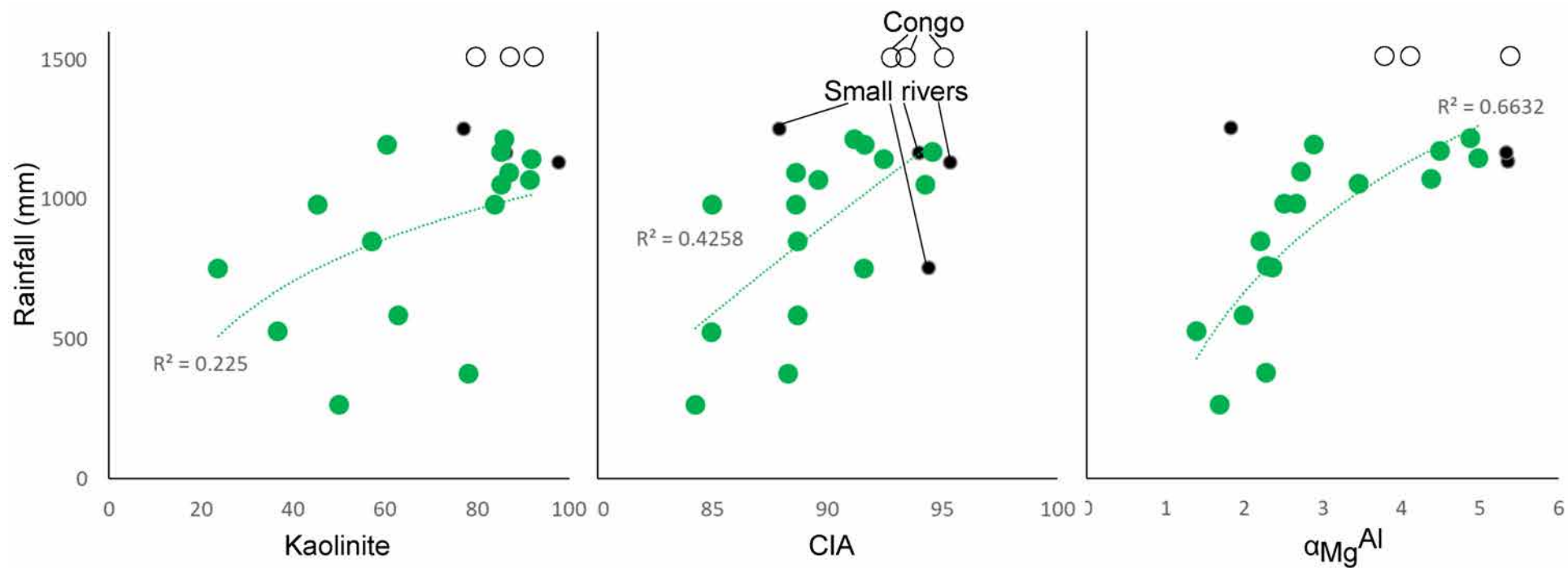












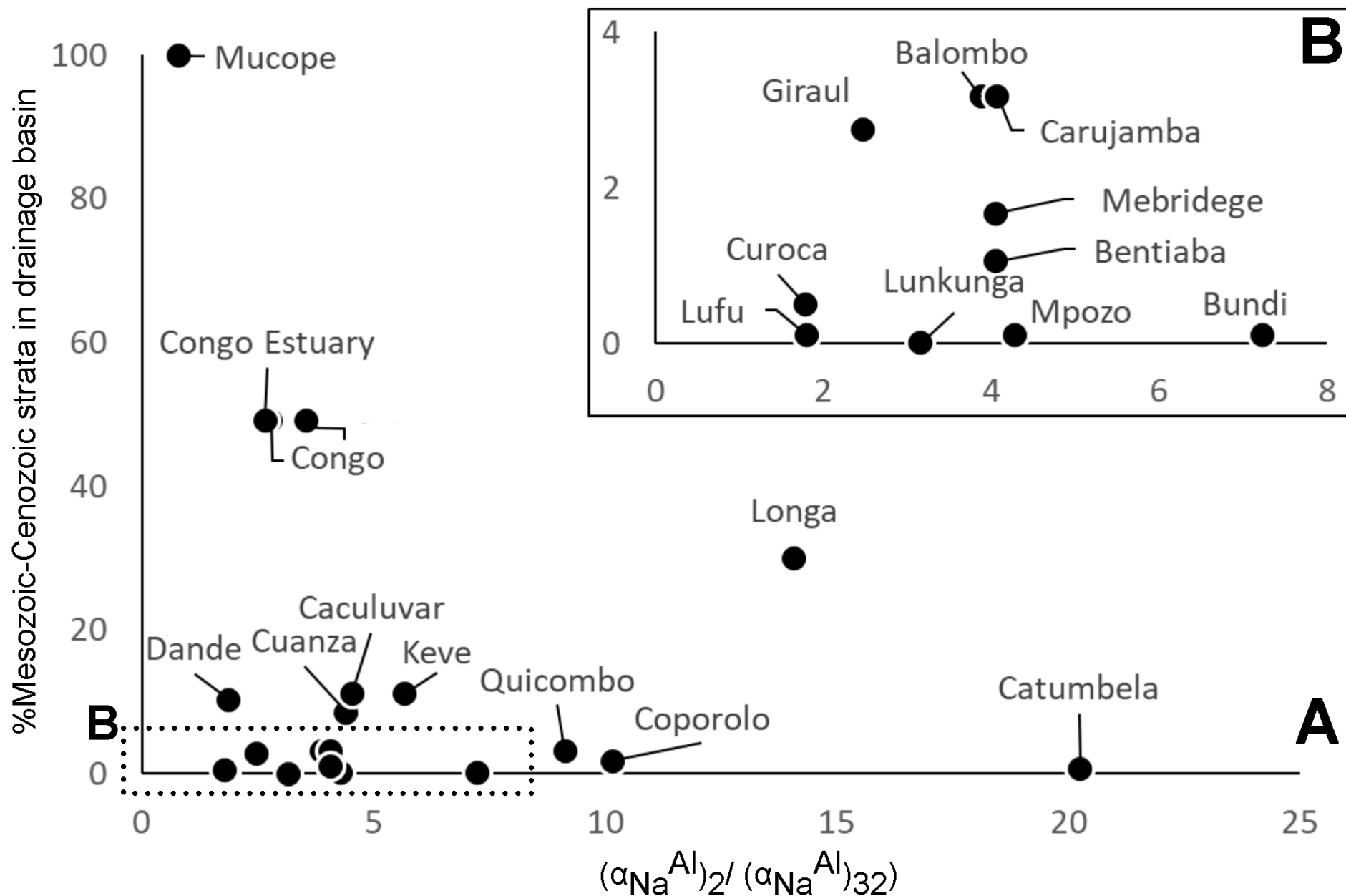


Table 1. A selection of compositional parameters that may reflect weathering intensity. (1) Use molar proportions; (2) Uses monocationic millimoles.

Parameter	Formula (when necessary); Response to weathering	Reference
Geochemical		
WIP (Weathering Index of Parker)	$(\text{CaO}^*/0.7+2\text{Na}_2\text{O}/0.35+2\text{K}_2\text{O}/0.25+\text{MgO}/0.9) \times 100$ (1); Decreases	Parker (1970)
CIA (Chemical Index of Alteration)	$\text{Al}_2\text{O}_3 / (\text{Al}_2\text{O}_3+\text{K}_2\text{O}+\text{CaO}^*+\text{Na}_2\text{O}) \times 100$ (1); Increases	Nesbitt and Young (1982)
CIW	$\text{Al}_2\text{O}_3 / (\text{Al}_2\text{O}_3+\text{CaO}+\text{Na}_2\text{O}) \times 100$ (1); Increases	Harnois (1988)
PIA	$(\text{Al}_2\text{O}_3-\text{K}_2\text{O}) / (\text{Al}_2\text{O}_3+\text{K}_2\text{O}+\text{Na}_2\text{O}) \times 100$ (1); Increases	Fedo et al. (1995)
Th/U	Increases if Th/U>4	McLennan et al. (1995), Gu et al. (2002)
Th/K	Increases	Deconinck et al (2003)
α_{ME}	$(\text{ImE}/\text{ME})_{\text{sample}}/(\text{ImE}/\text{ME})_{\text{UCC}}$, being ME a mobile element (Mg, Ca, Na, Sr, K, Ba) and ImE a non-mobile element with similar magmatic compatibility (Al for Mg, Ti for Ca, Sm for Na, Nd for Sr, and Th for K and Ba); Increases	Gaillardet et al. (1999)
K/Na and Rb/Sr	Increases	Yang et al. (2004)
Cs/Ti and Rb/Ti	Decreases	Yan et al. (2007)
W in M-F-W diagram	Long formulation (see cited reference); Progress towards vertex W of M-F-W ternary diagram	Ohta and Arai (2007)
Rb/K	Increases	Roy et al. (2008)
CPA	$\text{Al}_2\text{O}_3 / (\text{Al}_2\text{O}_3+\text{Na}_2\text{O}) \times 100$ (1); Increases	Buggle et al. (2011)
4Si in M+-4Si-R2+ diagram	Long formulation (see cited reference) (2); Progress towards vertex 4Si of M+-4Si-R2+ ternary diagram	Meunier et al. (2012)
$\alpha_{\text{E}}^{\text{Al}}$	$(\text{Al}/\text{E})_{\text{sample}}/(\text{Al}/\text{E})_{\text{UCC}}$, being E a mobile element; Increases	Garzanti et al. (2013a)
MIA _(o) (Mafic Index of Alteration for oxidative weathering)	$(\text{Al}_2\text{O}_3+\text{Fe}_2\text{O}_3) \times 100 / (\text{Al}_2\text{O}_3+\text{K}_2\text{O}+\text{CaO}^*+\text{Na}_2\text{O}+\text{MgO})$; Increases	Babechuck et al. (2014)
MIA _(r) (Mafic Index of Alteration for reduced weathering)	$(\text{Al}_2\text{O}) \times 100 / (\text{Al}_2\text{O}_3+\text{K}_2\text{O}+\text{CaO}^*+\text{Na}_2\text{O}+\text{MgO}+\text{FeO})$; Increases	Babechuck et al. (2014)
CIX (modified CIA)	$\text{Al}_2\text{O}_3 / (\text{Al}_2\text{O}_3+\text{K}_2\text{O}+\text{Na}_2\text{O}) \times 100$ (1); Increases	Garzanti et al. (2014)
Mineralogical		
Kaolinite proportion	Increases	E.g., Chamley (1989), Velde (1996)
MIA (Mineralogical Index of Alteration)	$\text{Quartz}\% / (\text{Quartz}\%+\text{Feldspar}\%) \times 100$; Increases	Rieu et al. (2007); Hessler et al. (2017)